

Electronic Supplementary Information:

Iron Carbide or Iron Carbide / Cobalt Nanoparticles for Magnetically-Induced CO₂ Hydrogenation over Ni/SiAlO_x Catalysts

Sumeet Suresh Kale, Juan M. Asensio, Marta Estrader, Mayke Werner, Alexis Bordet, Deliang Yi,
Julien Marbaix, Pier-Francesco Fazzini, Katerina Soulantica and Bruno Chaudret

Table of content:

ESI-1. Experimental section.	2
ESI.2. Characterization of <i>Ni/SiAlO_x</i>	7
ESI.3. Characterization of the Fe(0) NPs.....	9
ESI.4. Characterization of the NPs FeC-1 (SAR ~1100 W·g ⁻¹).....	11
ESI.5. Characterization of the NPs FeC-2 (SAR ~2100 W·g ⁻¹).....	13
ESI.6. Characterization of Co NRs.....	15
ESI.7. Characterization of the catalysts FeC-1/Ni and FeC-2/Ni	16
ESI.8. Effect of the residence time or weight hour space velocity (WHSV) on the reaction.....	17
ESI.9. Characterization of the catalyst FeC-1/Ni after the catalysis.	18
ESI.10. Characterization of Ni-pre	19
ESI.11. Characterization of the catalyst FeC-1/Ni-pre	21
ESI.12. Characterization of the catalyst FeC-2/Ni after catalysis.....	23
ESI.13. Characterization of Co/Ni and Co-FeC-1/Ni	24
ESI.14. Image of the continuous flow reactor.	26
ESI.15. Bibliography.	27

ESI-1. Experimental section.

ESI-1.1. Materials and Methods

All syntheses of non-commercial compounds were performed under argon atmosphere either by using Schlenk techniques or in a glove box. Mesitylene, toluene and tetrahydrofuran were obtained from VWR Prolabo, then purified on alumina desiccant and degassed by bubbling Ar through the solution for 20 minutes. They were then introduced in the glove-box. Hexadecylamine (HDA, 99%) and palmitic acid (PA, 99%) were obtained from Sigma-Aldrich. Lauric acid (LA) 99% was obtained from Acros. $[\text{Fe}\{\text{N}(\text{SiMe}_3)_2\}_2]_2$, $[\text{Co}\{\text{N}(\text{SiMe}_3)_2\}_2(\text{thf})]$ (thf = tetrahydrofurane) and $(\text{Ni}(\text{COD})_2)$ (COD = 1,5-cyclooctadiene) were obtained from Nanomeps. SiRALOx 5/320 was obtained from SASOL. All these compounds were stored in the glove-box and used without any additional purification.

The size and the morphology of the NPs were studied by transmission electronic microscopy (TEM). TEM grids were prepared by deposition of one drop of a colloidal solution containing the NPs on a copper grid covered with amorphous carbon. Conventional bright-field images were performed using JEOL microscopes (Model 1011 and 1400) working at 100 kV and 120 kV respectively. STEM and EDX analyses were performed using a Probe Corrected JEOL JEM-ARM200F Cold FEG equipped with a High Angle EDX detector working at 200 kV. XRD measurements were performed on a PANalytical Empyrean diffractometer using Co-K α radiation ($\lambda=0.1789$ nm) at 45 kV and 40 mA. Magnetic measurements were performed on a Vibrating Sample Magnetometer (VSM, Quantum Device PPMS Evercool II). Thermogravimetric analyses (TGA) were performed in a TGA/DSC 1 STAR System equipped with an ultra-microbalance UMX5, a gas switch GC200 and sensors DTA and DSC. XRD and VSM studies were carried out on compact powder samples that were prepared and sealed under argon atmosphere. ICP measurements were performed at KOLBE Mikroanalytisches Laboratorium. SAR measurements were performed by calorimetry experiments following the protocol already described in our previous work,¹ using a coil with a fixed frequency of 93 kHz (see Supporting Info for more details). Gas Chromatography–Mass Spectrometry analyses were performed on a PerkinElmer 580 Gas Chromatograph coupled to a Clarus SQ8T Mass Spectrometer.

ESI-1.2. Synthesis of Fe(0) Nanoparticles

Fe (0) nanoparticles were synthesized by following a method reported by our group.^{1, 2} In a typical synthesis, 2.62 mmol of PA (666.4 g) and 2.00 mmol of HDA (483.0 mg) were dissolved in the mesitylene and added to a green solution of 1.00 mmol of $[\text{Fe}\{\text{N}(\text{SiMe}_3)_2\}_2]_2$ (753.2 mg) in 10 ml of mesitylene in a Fischer Porter bottle in the glove box. The Fischer Porter bottle was then pressurized with hydrogen gas (2

bar) and placed in an oil bath at 150 °C for 72 h under vigorous magnetic stirring (400 rpm). After 72 h the reaction was stopped, and the NPs were recovered by decantation assisted by a magnet. The NPs were further washed with toluene (3×10 mL) and THF (3×10 mL) and dried under vacuum to give ~100 mg of Fe(0) NPs as a powder which contained 75% of Fe as determined by TGA (Yield in Fe – 67%).

ESI-1.3. Synthesis of FeC-1 and FeC-2 (Fe_{2.2}C NPs)

Iron carbide NPs were prepared through carbidization of preformed Fe (0) NPs. In a typical experiment, in the glove box, Fe(0) NPs (50 mg, ~0.67 mmol of iron) were dispersed in mesitylene (10 mL) in a Fischer Porter bottle. The heating power of the FeC NPs was controlled by controlling the amount of ligand at the beginning of the reaction, following a previously reported procedure.³ Thus, for **FeC-1** NPs with a SAR value of ~1100 W·g⁻¹, 30 mg of a 1:1 mixture of palmitic acid and hexadecylamine were added at the beginning of the reaction, and for **FeC-2** NPs with a SAR value of ~2000 W·g⁻¹, 50 mg of palmitic acid were added instead. The mixtures were then pressurized with CO and H₂ (2 bar of each), and were allowed to stir (700 rpm) at 150 °C for 120 h. At the end of the reaction, the NPs were recovered by decanting the supernatant solution with the help of a magnet. The recovered NPs were washed with toluene (3×5 mL) and dried under vacuum to give ~50 mg of Fe_{2.2}C NPs as a powder which Fe content determined by TGA was of ~70 wt% in all the cases. (Yield in Fe – 84%)

ESI-1.4. Synthesis of Co-NRs

Cobalt nanorods were synthesized by slightly modifying an earlier reported procedure.⁴ In a Fischer-Porter reactor a solution of HDA (818.5 mg, 3.4 mmol in 22 mL toluene) was mixed with a solution of LA (420.3 mg, 2.10 mmol in 16 mL toluene) leading to the formation of a white viscous liquid due to the formation of the acid-amine salt is finally dissolved. After 3 min, a solution of [Co{N(SiMe₃)₂}(thf)] (902.2 mg, 2 mmol in 2 mL toluene) was added rapidly giving rise to a blue solution. The reactor was transferred to a vacuum line connected to a H₂ source, and after removing the Ar under vacuum, the bottle was pressurized with 3 bar of H₂ and let under stirring for 7 min. Then, the mixture was heated in an oil bath at 110°C for 24 h. The reactor was cooled down and transferred into the glove-box. The black precipitate was separated from the dark brown supernatant solution and it was washed repeatedly with toluene in order to remove the excess of ligands and the spherical nanoparticles that are produced together with the nanorods. The black precipitate was finally washed with pentane and dried in the glove-box. This synthesis typically yields Co-NRs of 80-90 nm. The Co content was determined from VSM measurements after verification by FC-ZFC hysteresis measurements that they were not oxidized (no exchange bias after FC) and knowing that they present the same saturation magnetization (M_s) as for Co-bulk (M_s = 162 emu/g).⁵

The Co content can vary from batch to batch from 80 to 95% (%w) resulting to a final Co yield of about 65%. The real amount of Co obtained by the magnetic measurements was considered when fixing the amounts of other reactants.

ESI-1.5. Synthesis of Ni doped SiRAIOx and Ni-pre

The catalyst (10 wt% of Ni supported on SiRAIOx) was prepared by decomposition Ni(COD)₂ on the support at 150 °C. Typically, SiRAIOx (1 g) was added to a yellow solution of Ni(COD)₂ (520.6 mg) in mesitylene (20 ml) in the glove box. The resulting mixture was sonicated for 20 min. and then stirred under Ar at room temperature for 30 minutes. The solution was then refluxed at 150°C for 1 h under rigorous stirring (700 rpm). At the end of the reaction, the Ni supported on SiRAIOx was recovered by decantation of supernatant solution, washed with THF (5 ml x 3 times) and dried under vacuum. Yield ~ 1 g Ni/SiRAIOx. **Ni/SiRAIOx**: Metal content determined by ICP (wt%): Ni, 9.86. For the preparation of **Ni-pre**, 500 mg of Ni/SiRAIOx were heated at 400 °C in the presence of a H₂ atmosphere for 1 h.

ESI-1.6. Synthesis of FeC/Ni/SiRAIOx

In a typical experiment in the glove box, **FeC-1** or **FeC-2** (60 mg, Fe content ca. 75%), were dispersed in toluene (10 ml). Then, Ni/SiRAIOx (400 mg) was added to the dispersion and the mixture was sonicated for 20 min. At the end, the excess of toluene was removed under vacuum. TEM pictures are given in the SI. Yield ~ 430 mg of FeC/Ni/SiRAIOx. Metal content determined by ICP (wt%): **FeC-1/Ni**: Fe, 9.57; Ni, 7.31. **FeC-2/Ni**: Fe, 8.92; Ni, 7.01. **FeC-1/Ni-pre**: Fe, 6.83; Ni, 6.37.

ESI-1.7. Synthesis of CoNRs/Ni/SiRAIOx

Co-NRs (60 mg, Co content ca. 90%), were dispersed in toluene (10 ml). Then, Ni/SiRAIOx (400 mg) was added to the dispersion and the mixture was sonicated for 20 min. At the end, excess of toluene was removed under vacuum. All the characterization data are given in the SI. Yield ~ 430 mg of CoNRs/Ni/SiRAIOx. Metal content determined by ICP (wt%): **Co/Ni**: Co, 9.57; Ni, 7.31.

ESI-1.8. Synthesis of CoNRs/FeC/Ni/SiRAIOx

Co-NRs (60 mg, Co content ca. 75%) were dispersed in toluene (10 ml). Then, Ni/SiRAIOx (300 mg) was added to the dispersion and the mixture was sonicated for 20 min. At the end, excess of toluene was removed under vacuum. After this, 100 mg of **FeC-1** supported on SiRAIOx powder were introduced in the

vessel and mixed manually. Yield ~ 420 mg of CoNRs/FeC/Ni/SiRAlOx Metal content determined by ICP (wt%): **Co-FeC-1/Ni**: Co, 6.60; Fe, 1.45; Ni, 5.86.

ESI-1.9. General catalytic conditions

The CO₂ hydrogenation activity of the prepared samples was evaluated in a glass reactor (ID 1 cm) with a H₂:CO₂ molar ratio of 4 in a continuous flow using a magnetic-induction coil supplied by Fives Celes working at a fixed frequency of 300 kHz. The coil is 3 cm wide and 2 cm high and has a volume of 14 mL (see Fig S32). The induction coil is equipped with a user interface, where the software permits to continuously monitor and adjust the percentage of magnetic field amplitude applied. The relation between the power in kW and the magnetic field amplitudes in % and mT is shown in the table below.

Field (%)	Power (kW)	Field amplitude (mT)
100	18.0	80
80	9.2	64
60	4.8	48
40	2.0	32
20	0.8	16

The total flow rate was set to 25 ml/min throughout the experiments. The reactor was loaded with 300, 400 or 600 mg of the catalyst and placed at the centre of the coil in order to maximize interaction with the magnetic field in magnetic heating experiments, or in the centre of the oven in conventional heating experiments. The temperature of catalyst bed was continuously monitored using infrared camera in magnetic heating experiments and using a Pt thermocouple in conventional heating. The thermal infrared camera (testo 885 model) was directly pointed at the glass reactor. The global temperature of the reactor increased from 25 to ca. 250-300 °C in 30 s (see Fig S34). Each value of the magnetic field amplitudes tested was kept for at least 45 minutes to assure that the equilibrium was achieved. The mixture of the exit gases was injected into the GC chromatograph, and the resulting chromatogram gave the product distribution in the gas phase. The conversions and yields were obtained after performing a balance for the C, considering the corresponding response factor after calibration of the TCD detector. Each value of conversion and yield was obtained as the average of 3 injections into the GC at the same magnetic field or oven temperature.

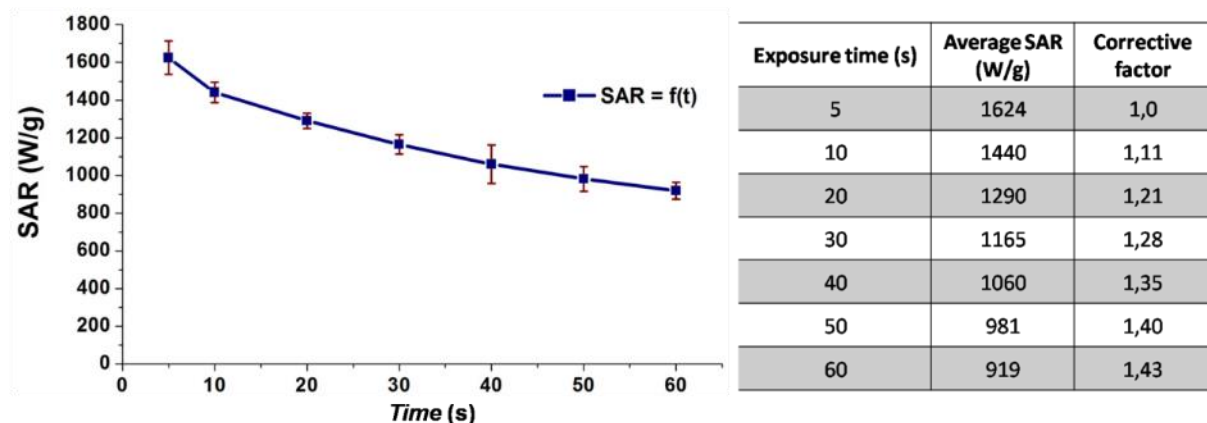
ESI-1.10. Hyperthermia measurements

For a typical hyperthermia experiment, an air-tight tube containing about 10 mg of iron carbide or iron/iron carbide nanocrystals dispersed in 0.5 ml of mesitylene was filled under inert atmosphere. The tube was then placed in a calorimeter containing 2.5 ml of deionized water, the temperature of which was monitored during the experiment. The calorimeter was exposed to an alternative magnetic field for a time varying between 10 and 40s so that the temperature rise never exceeded 20°C. The temperature rise at the end of the magnetic field application was always measured after shaking the calorimeter to ensure the temperature homogeneity, which was measured by two probes (at the top and the bottom of the calorimeter). The temperature rise was determined after this process from the mean slope of the $\Delta T/\Delta t$ function. Then the raw SAR values were calculated using the expression:

$$SAR = \frac{\sum_i C_{pi} m_i}{m_{Fe}} \times \frac{\Delta T}{\Delta t}$$

where C_{pi} and m_i are the specific heat capacity and the mass for each component respectively ($C_p = 449 \text{ J.kg}^{-1}.\text{K}^{-1}$ for $\text{Fe}_{2.2}\text{C}$ NPs, $C_p = 1750 \text{ J.kg}^{-1}.\text{K}^{-1}$ for mesitylene, $C_p = 4186 \text{ J.kg}^{-1}.\text{K}^{-1}$ for water and $C_p = 720 \text{ J.kg}^{-1}.\text{K}^{-1}$ for glass), and m_{Fe} is the mass of the pure iron carbide NPs.

The raw SAR values were corrected from the calorimeter losses, which were previously calibrated. For the calibration, a sample containing nanoparticles displaying moderate SAR was exposed for different time periods to an alternating magnetic field of 47 mT, 96 kHz. For each time, the SAR of the sample was measured. The SAR measured for an exposure time of 5s is considered as the “real” SAR (no losses). For longer exposure times, the difference between the measured SAR and the “real” SAR allows the determination of a corrective factor. The calibration curve is displayed below.



For each exposure time, the SAR was measured 3 times to ensure reproducibility. For the samples presented in this article, the measurement times were often comprised between 10 and 20s.

ESI.2. Characterization of *Ni/SiRAIOx*.

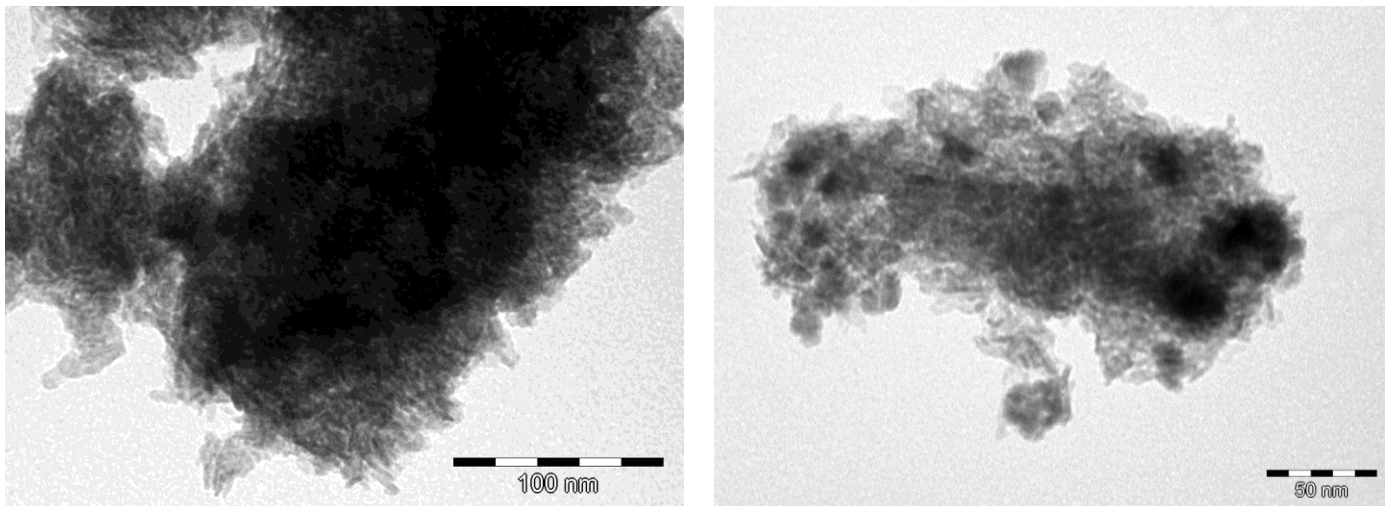


Figure S1. TEM images of *Ni/SiRAIOx* at different magnifications.

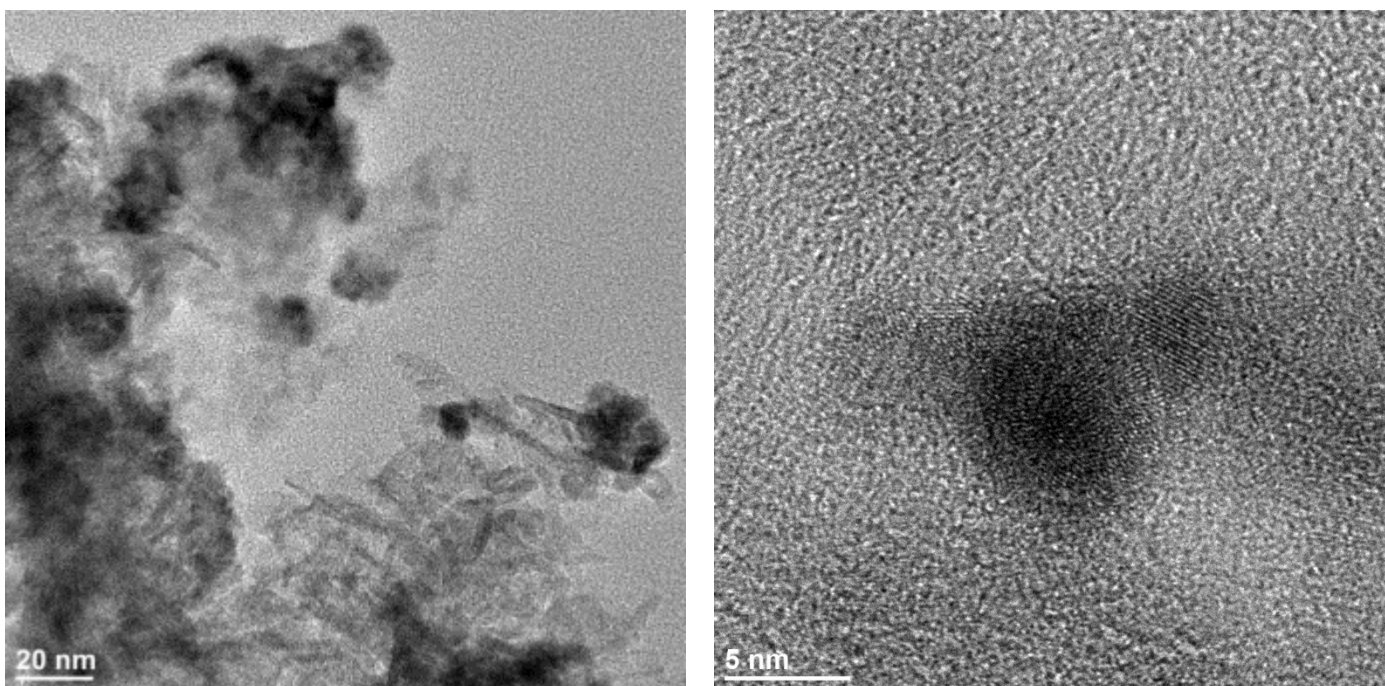


Figure S2. STEM-BF (Bright field) images of *Ni/SiRAIOx* at different magnifications.

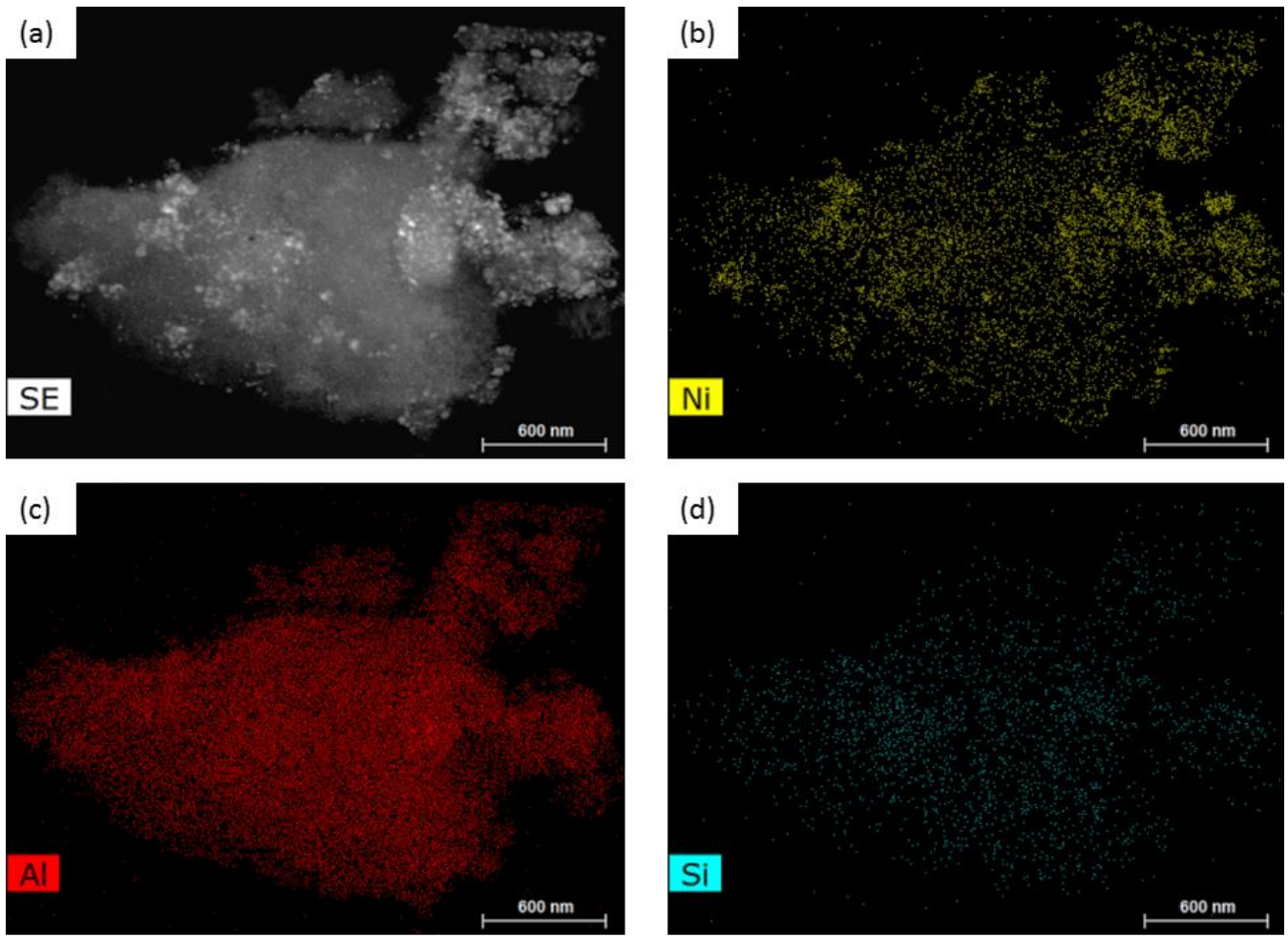


Figure S3. (a) STEM-HAADF (High angle annular dark field) images of **Ni/SiAlOx** and (b-d) EDX mapping of **Ni/SiAlOx** showing the elements (b) Ni, (c) Al and (d) Si.

ESI.3. Characterization of the Fe(0) NPs

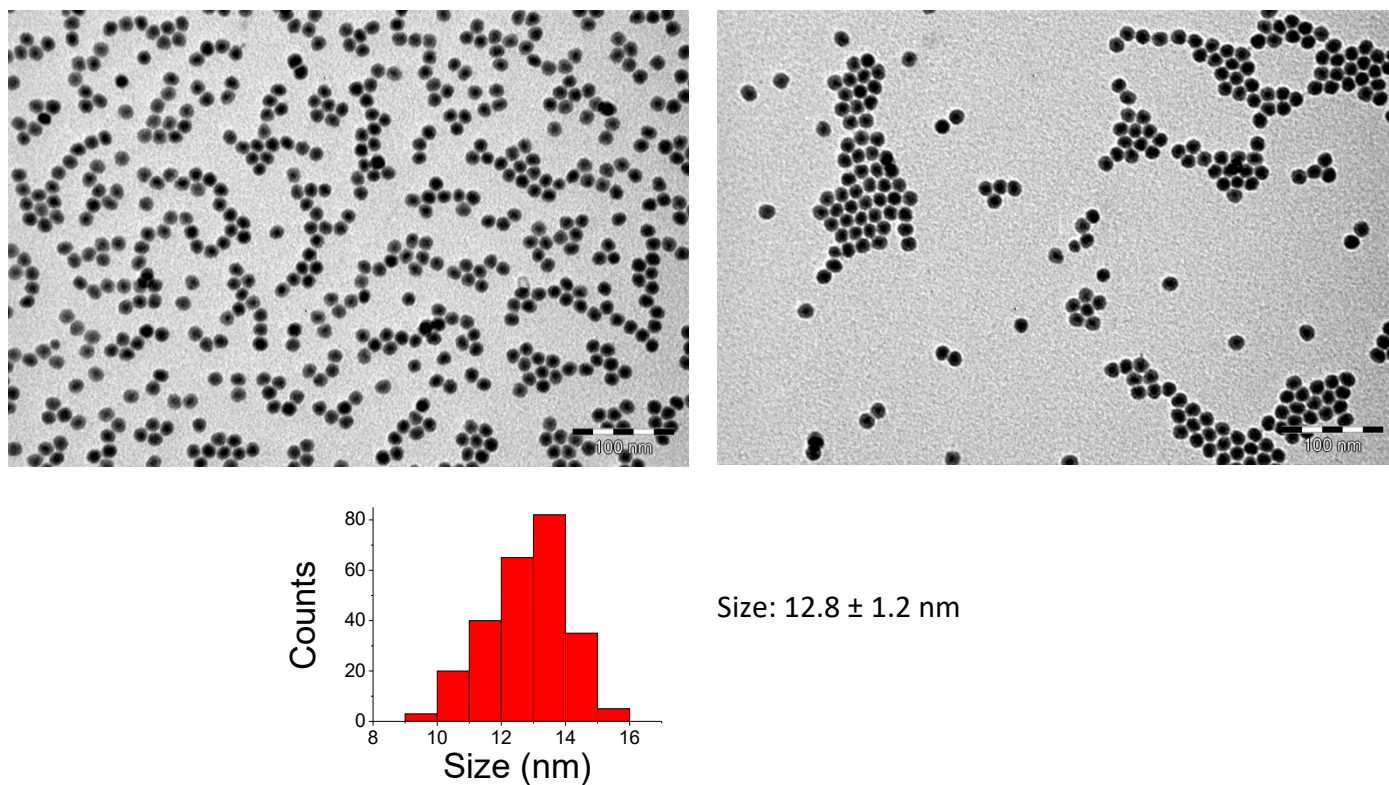


Figure S4. TEM images and size distribution of Fe(0) NPs and size distribution.

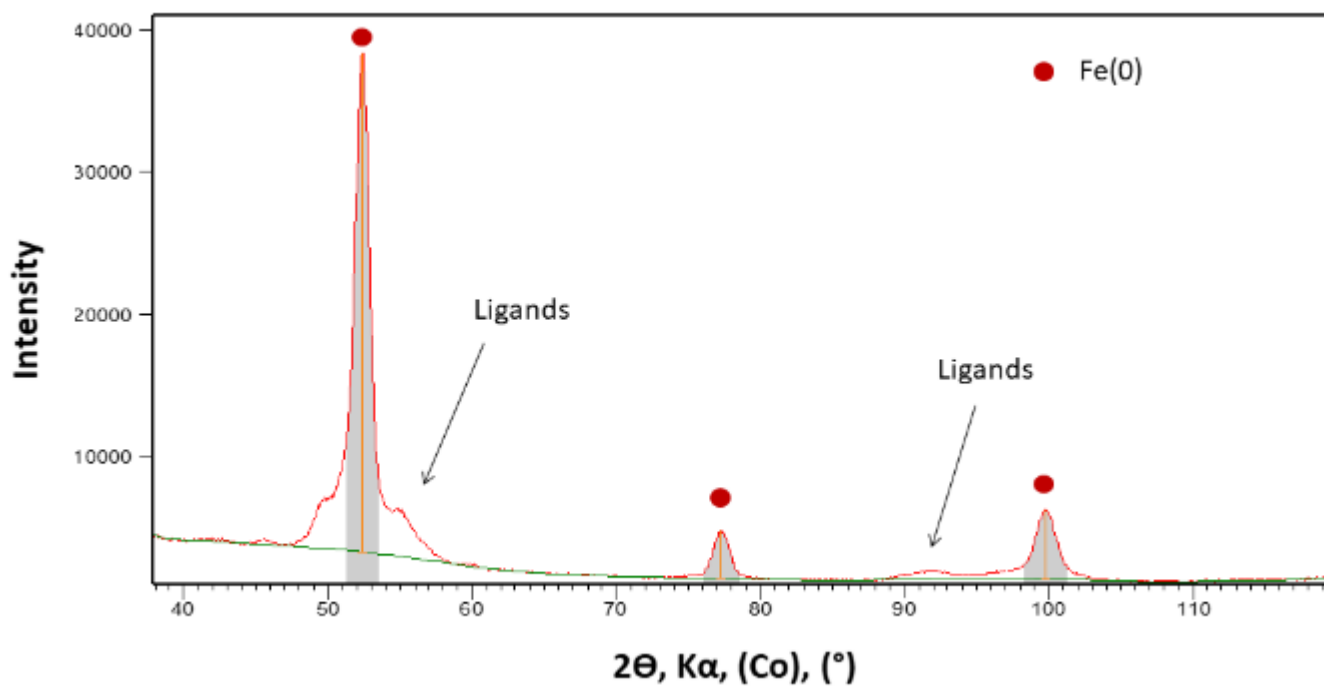


Figure S5. XRD diffractogram of Fe(0) NPs. The labelled peaks correspond to the Fe(0) phase.

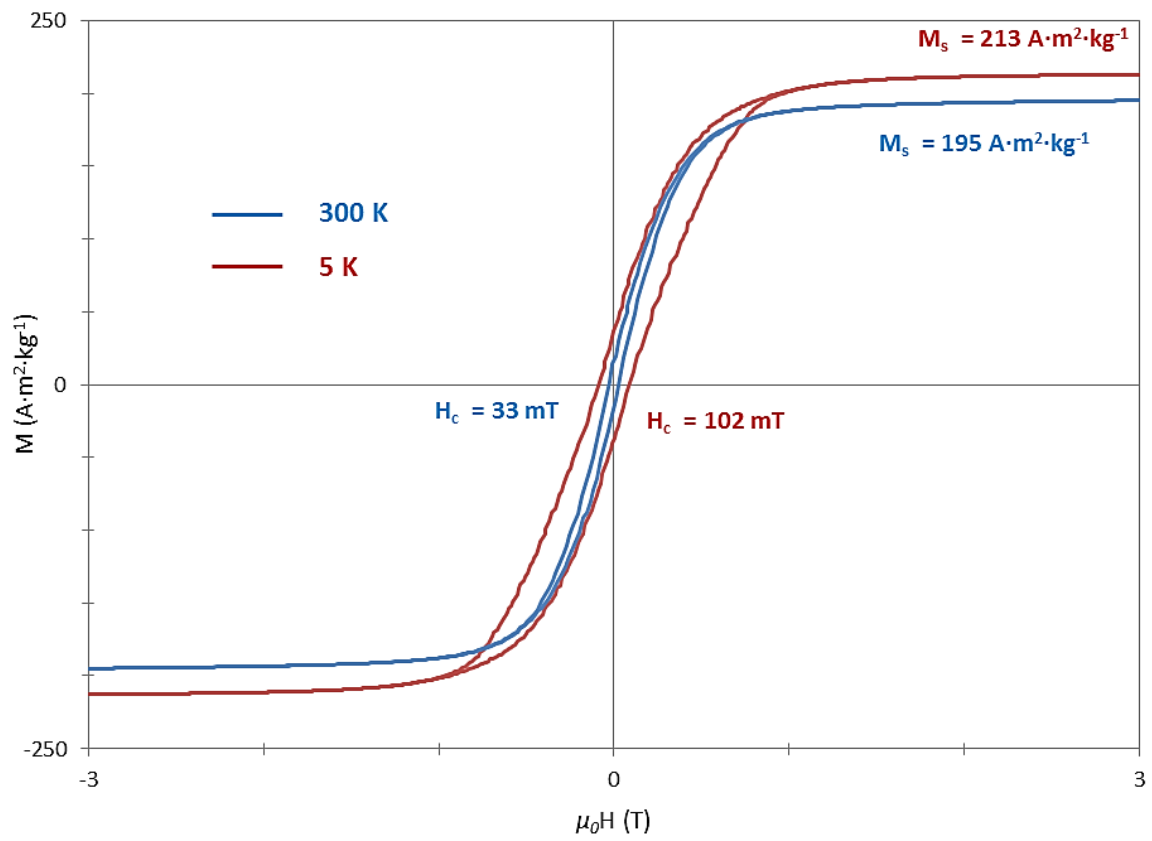


Figure S6. Hysteresis loops measured by VSM analysis for Fe(0) NPs at 300 K and 5 K

ESI.4. Characterization of the NPs *FeC-1* (SAR $\sim 1100 \text{ W}\cdot\text{g}^{-1}$)

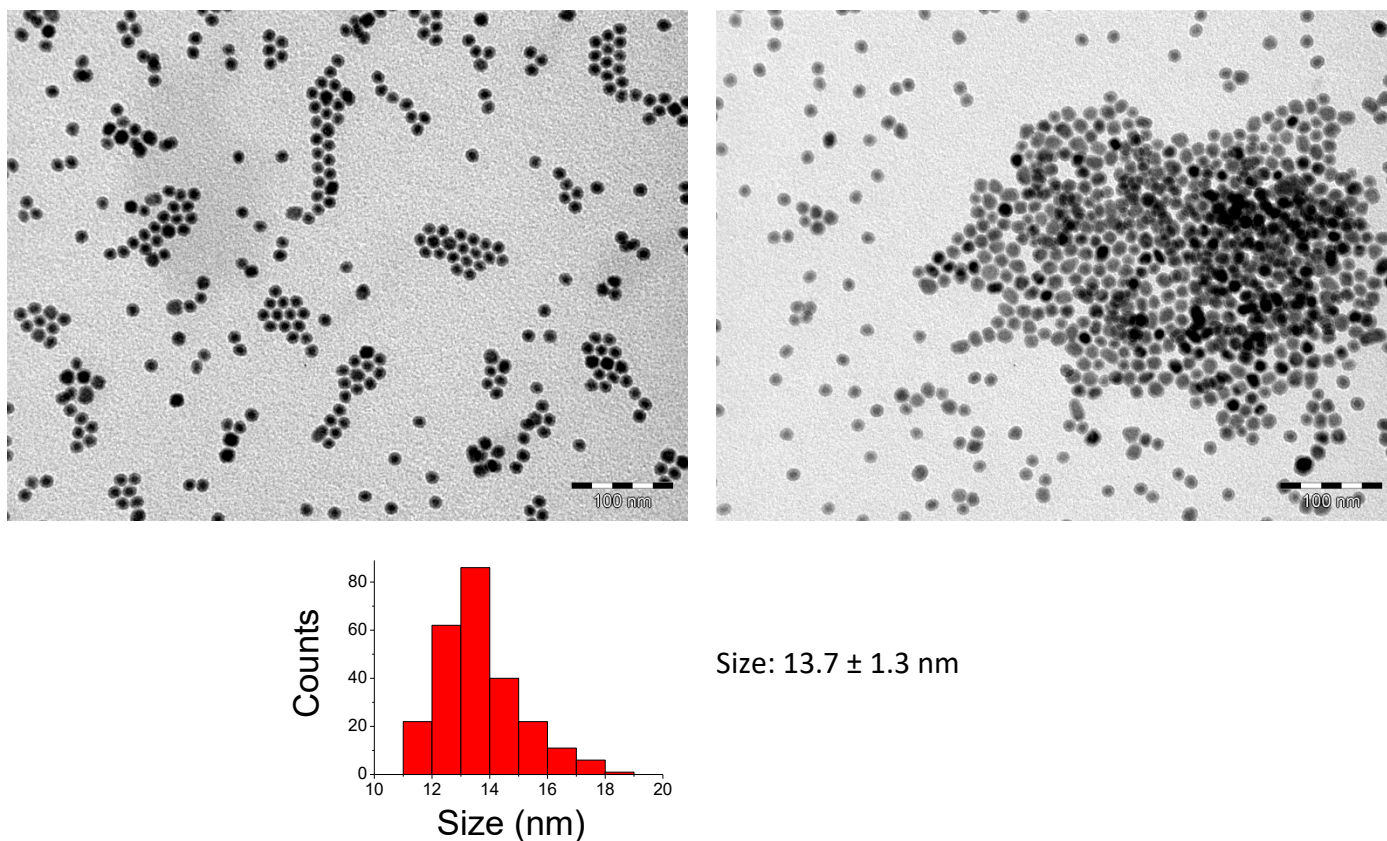


Figure S7. TEM images and size distribution of NPs **FeC-1** and size distribution.

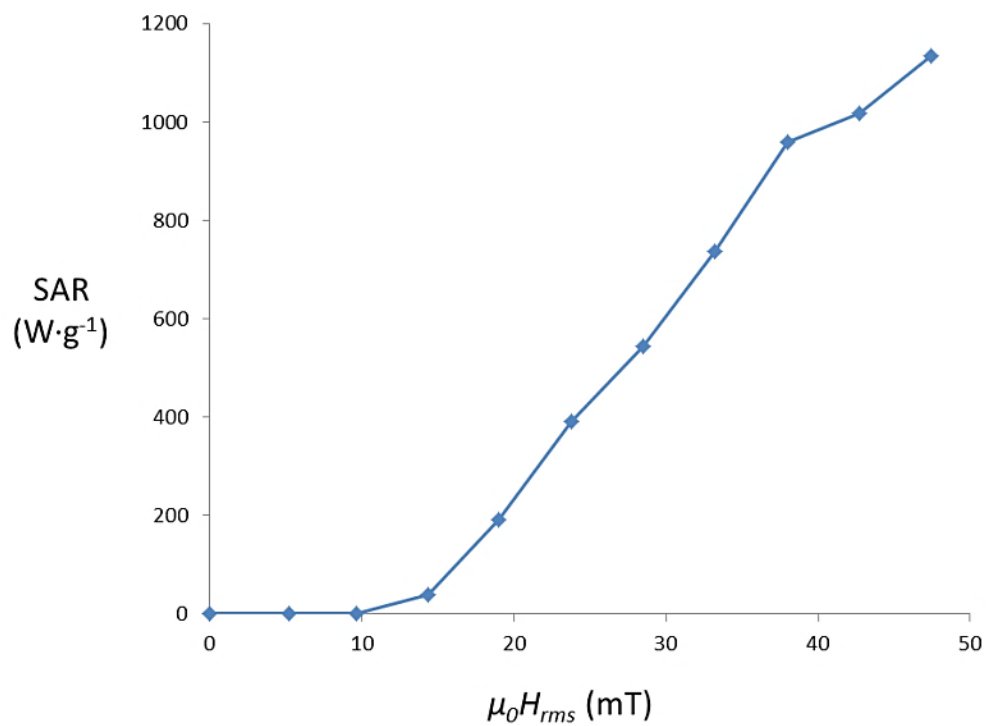


Figure S8. Specific absorption rate (SAR) for NPs **FeC-1** at different $\mu_0 H_{rms}$ measured at a f of 96 kHz.

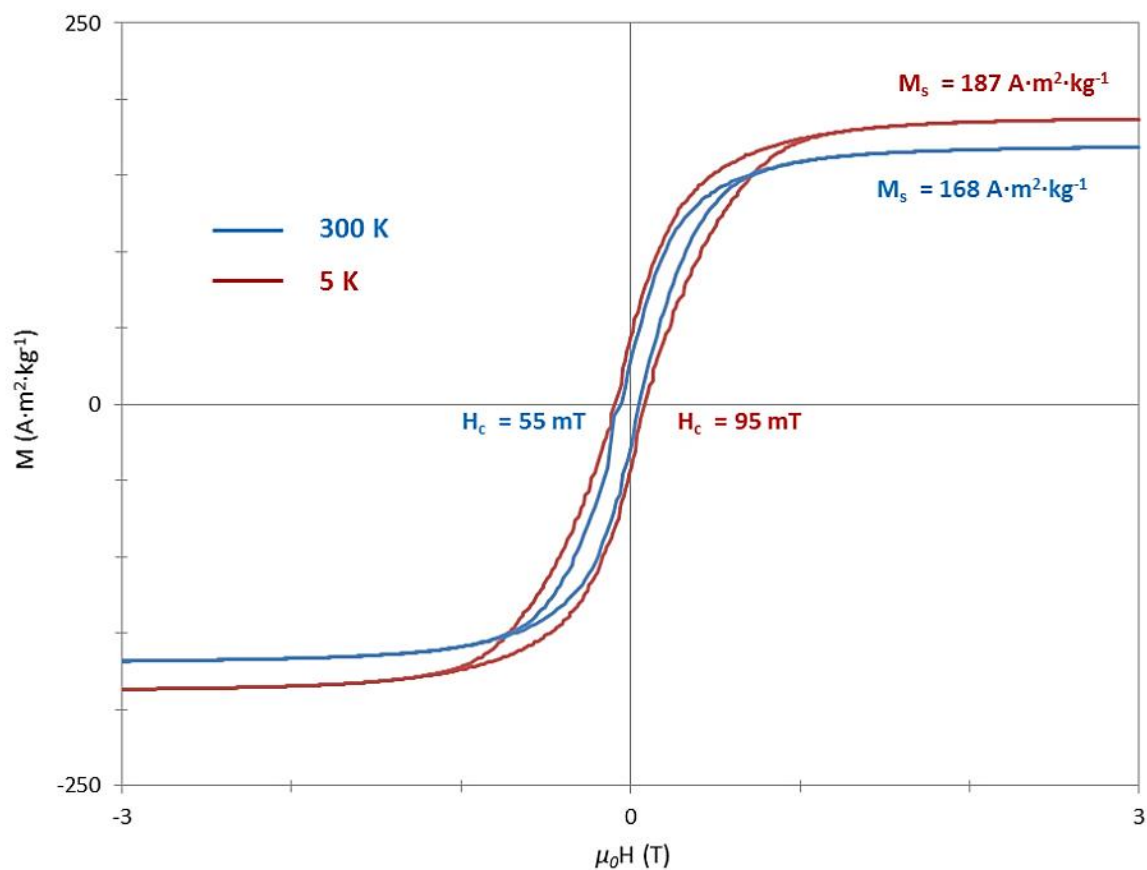


Figure S9. Hysteresis loops measured by VSM analysis for NPs FeC-1 at 300 K and 5 K

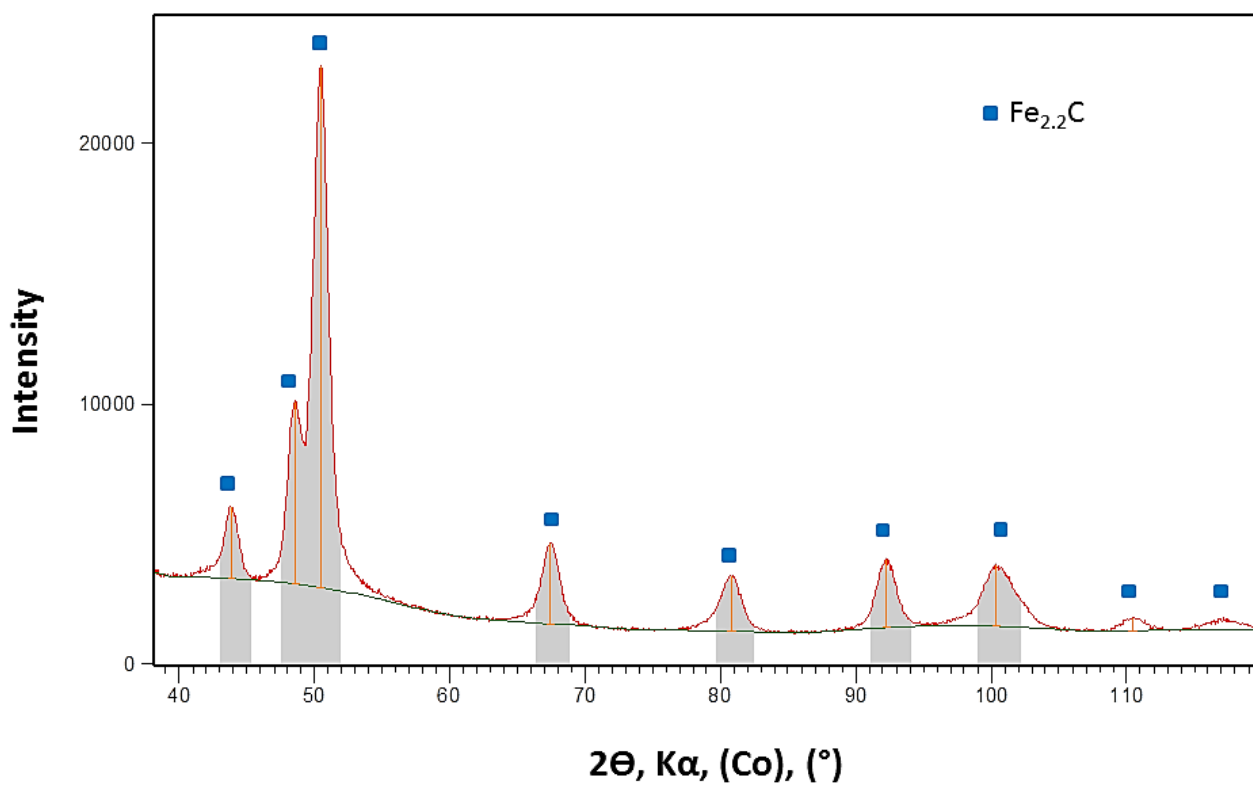


Figure S10. XRD diffractogram of NPs FeC-1. The peaks labelled in blue correspond to the $\text{Fe}_{2.2}\text{C}$ phase.

ESI.5. Characterization of the NPs FeC-2 (SAR $\sim 2100 \text{ W}\cdot\text{g}^{-1}$)

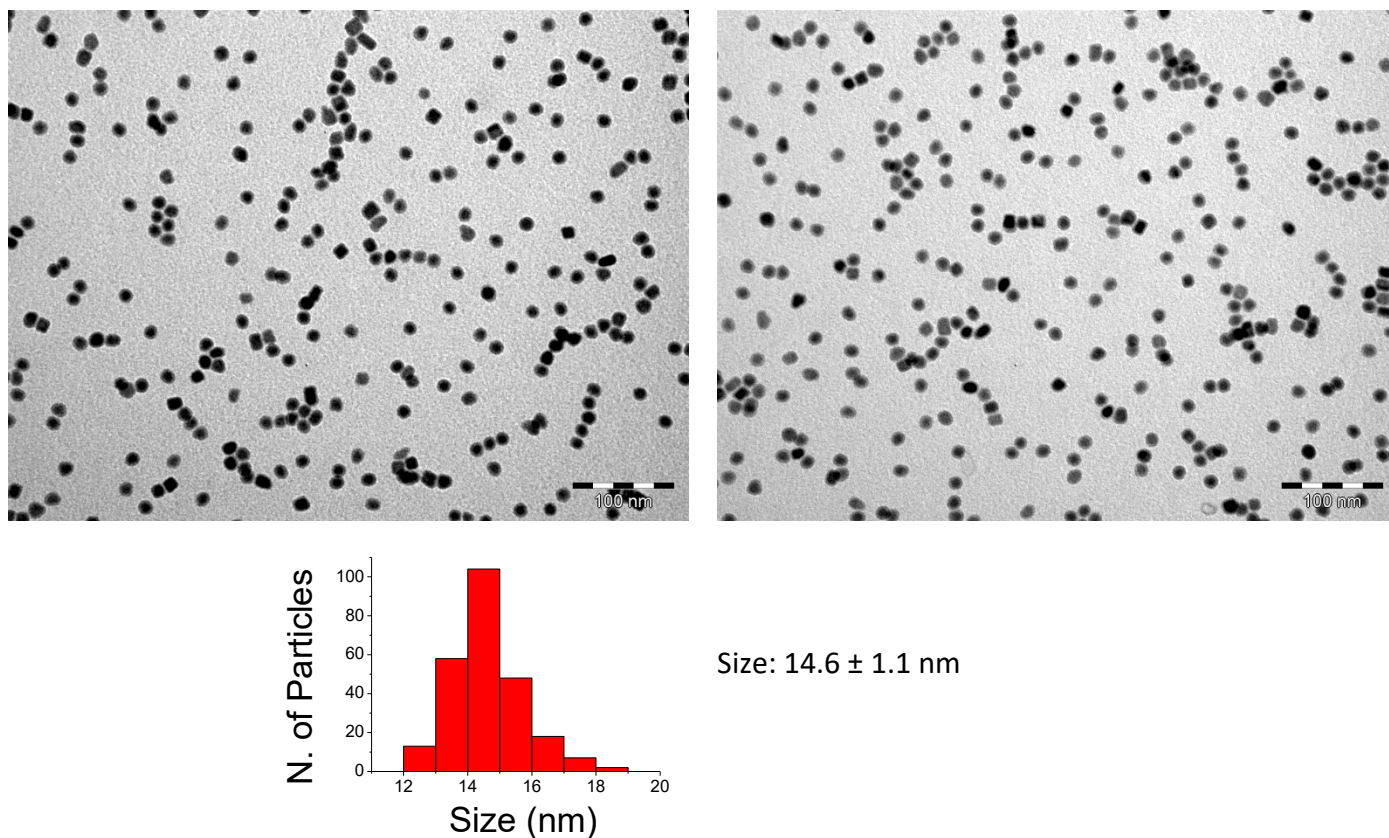


Figure S11. TEM images and size distribution of NPs FeC-2 and size distribution.

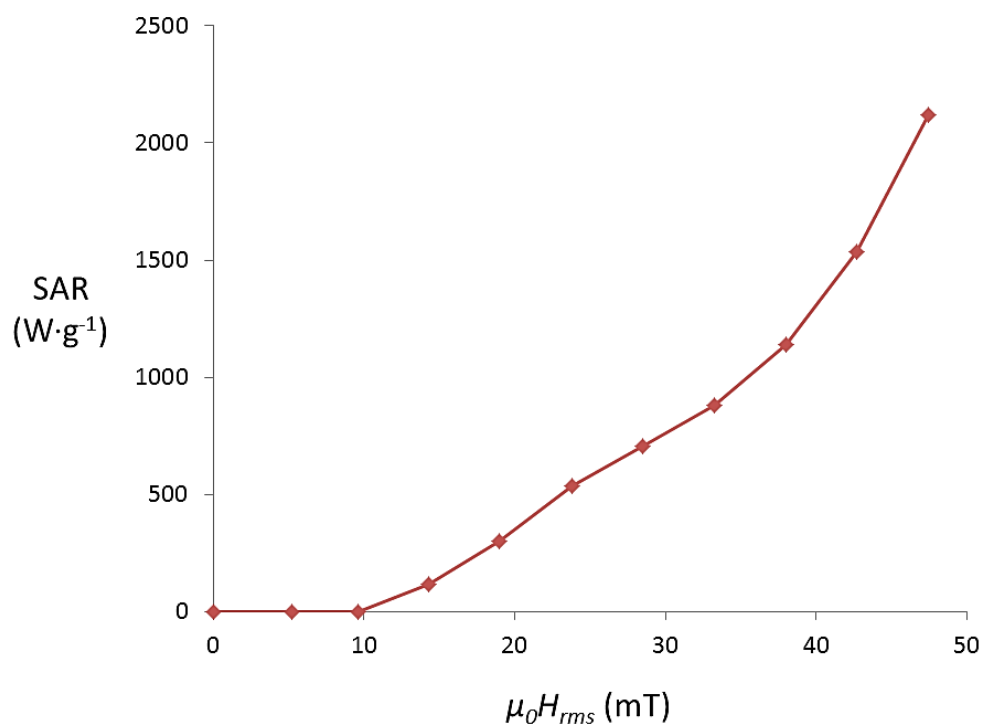


Figure S12. Specific absorption rate (SAR) for NPs FeC-2 at different $\mu_0 H_{rms}$ measured at a f of 96 kHz.

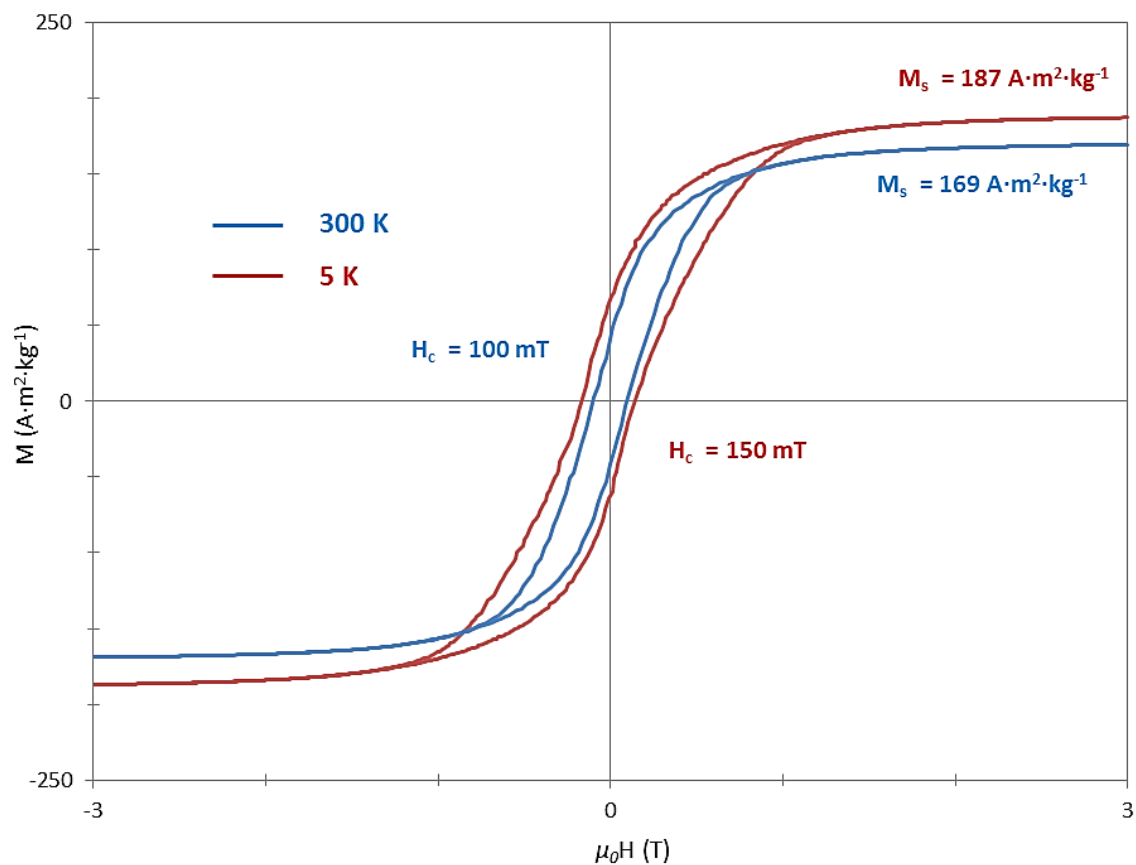


Figure S13. Hysteresis loops measured by VSM analysis for NPs FeC-2 at 300 K and 5 K

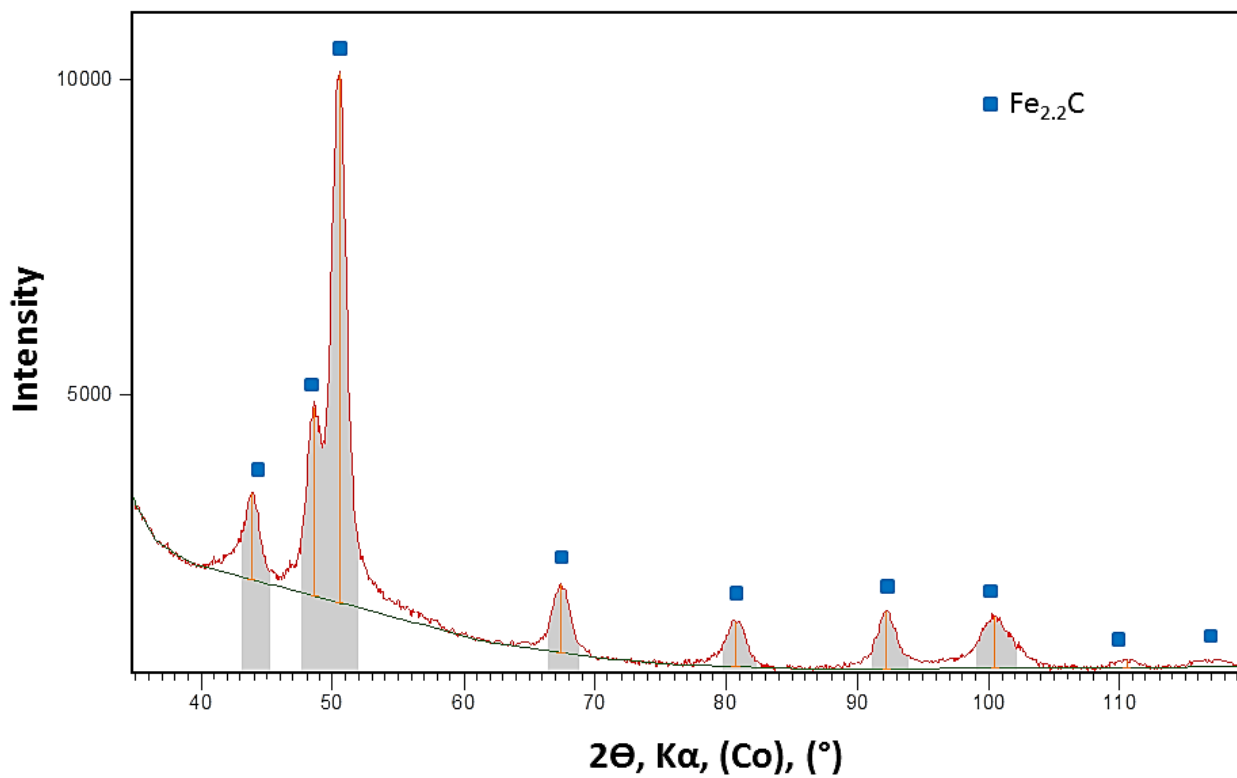


Figure S14. XRD diffractogram of NPs FeC-2. The peaks labelled in blue correspond to the $\text{Fe}_{2.2}\text{C}$ phase.

ESI.6. Characterization of Co NRs

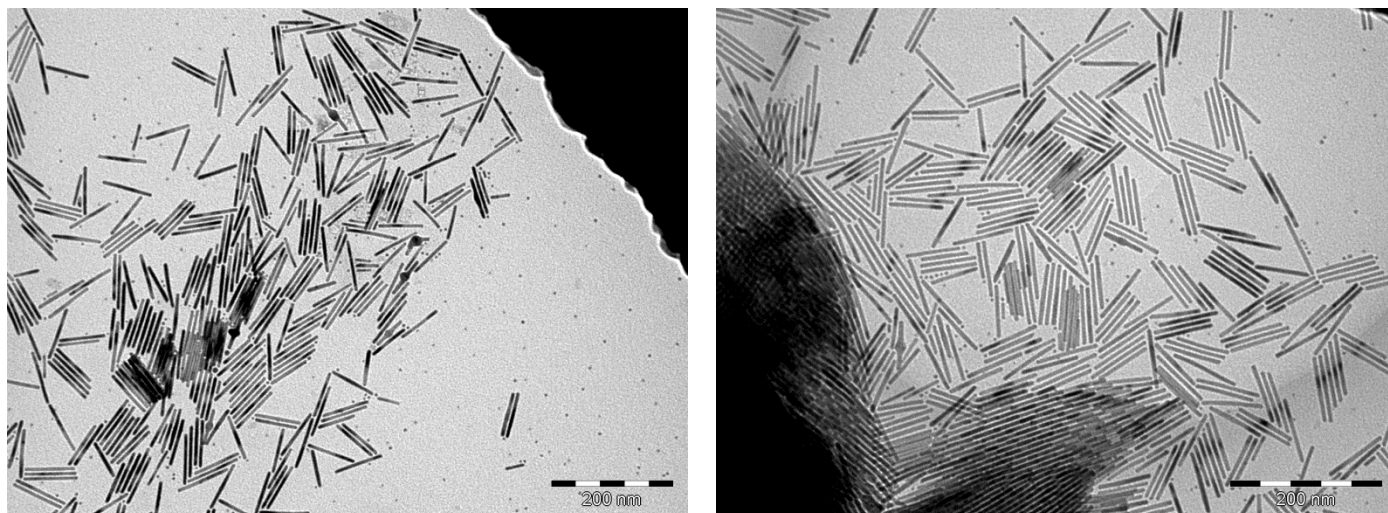


Figure S15. TEM images of Co NRs at different magnifications.

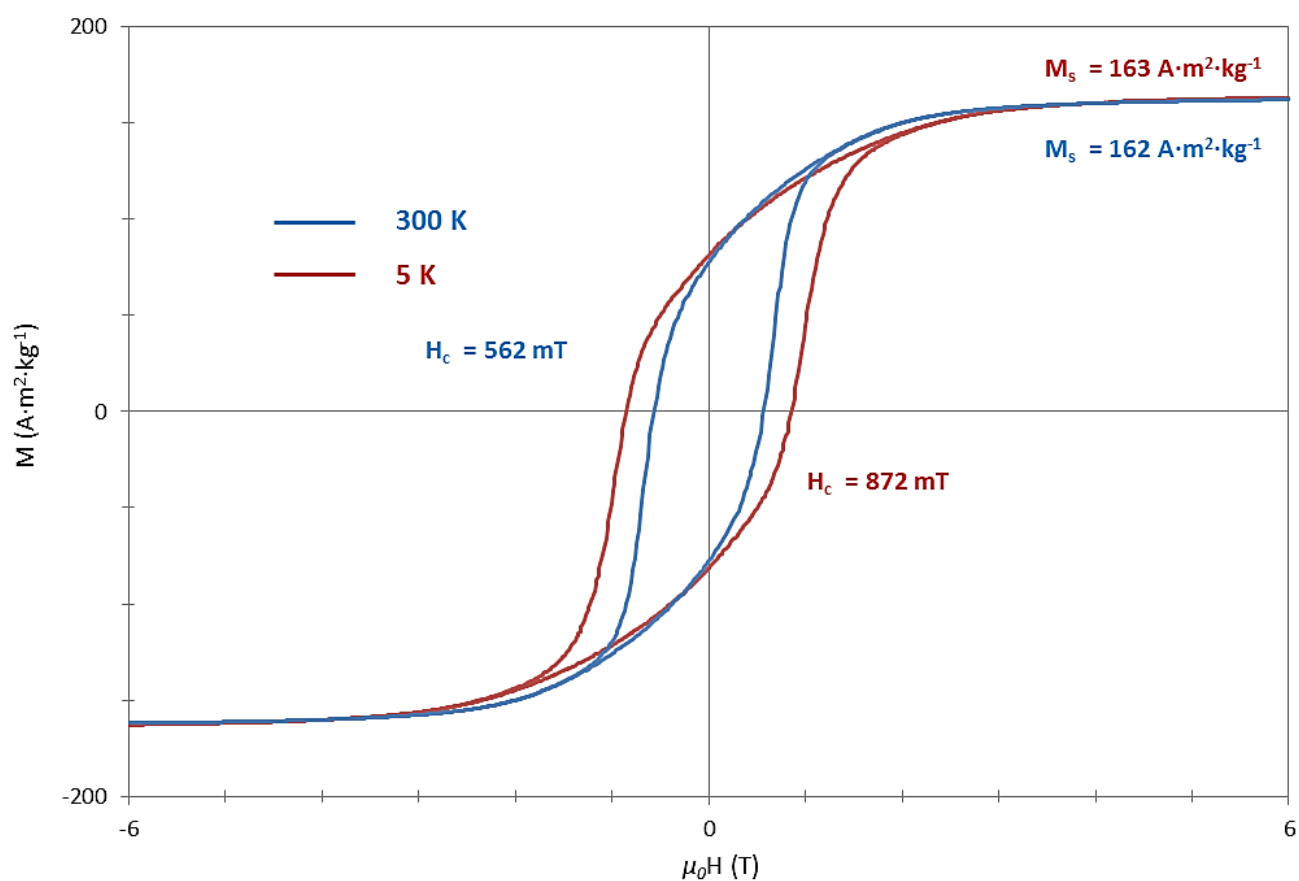


Figure S16. Hysteresis loops measured by VSM analysis for Co NRs at 300 K and 5 K

ESI.7. Characterization of the catalysts *FeC-1/Ni* and *FeC-2/Ni*

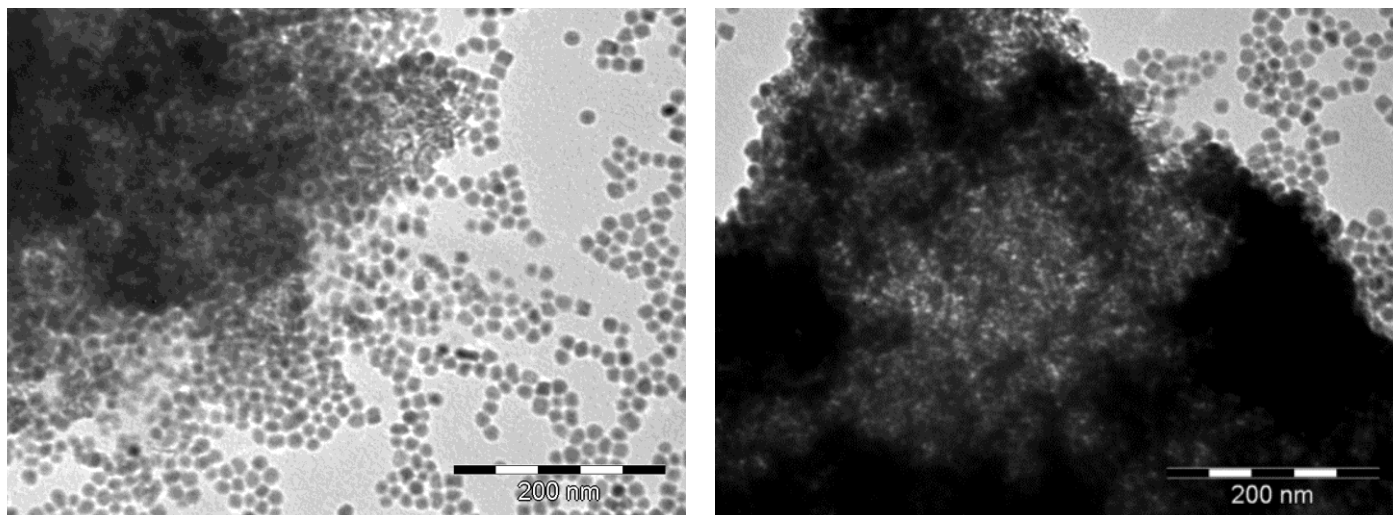


Figure S17. TEM images of *FeC-1/Ni*.

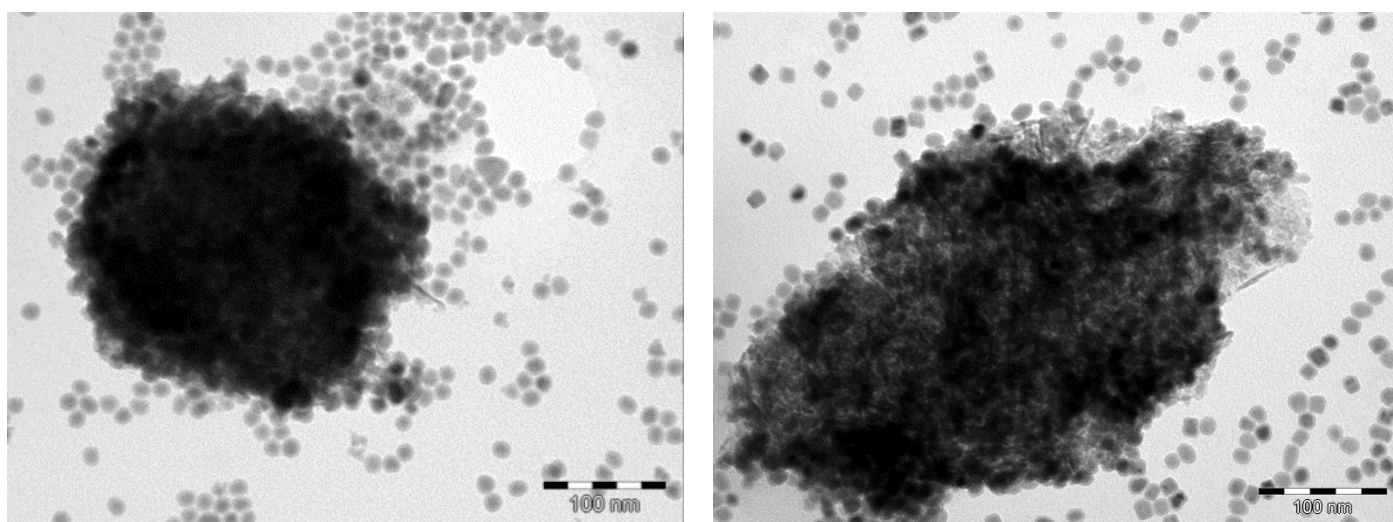


Figure S18. TEM images of *FeC-2/Ni*.

ESI.8. Effect of the residence time or weight hour space velocity (WHSV) on the reaction.

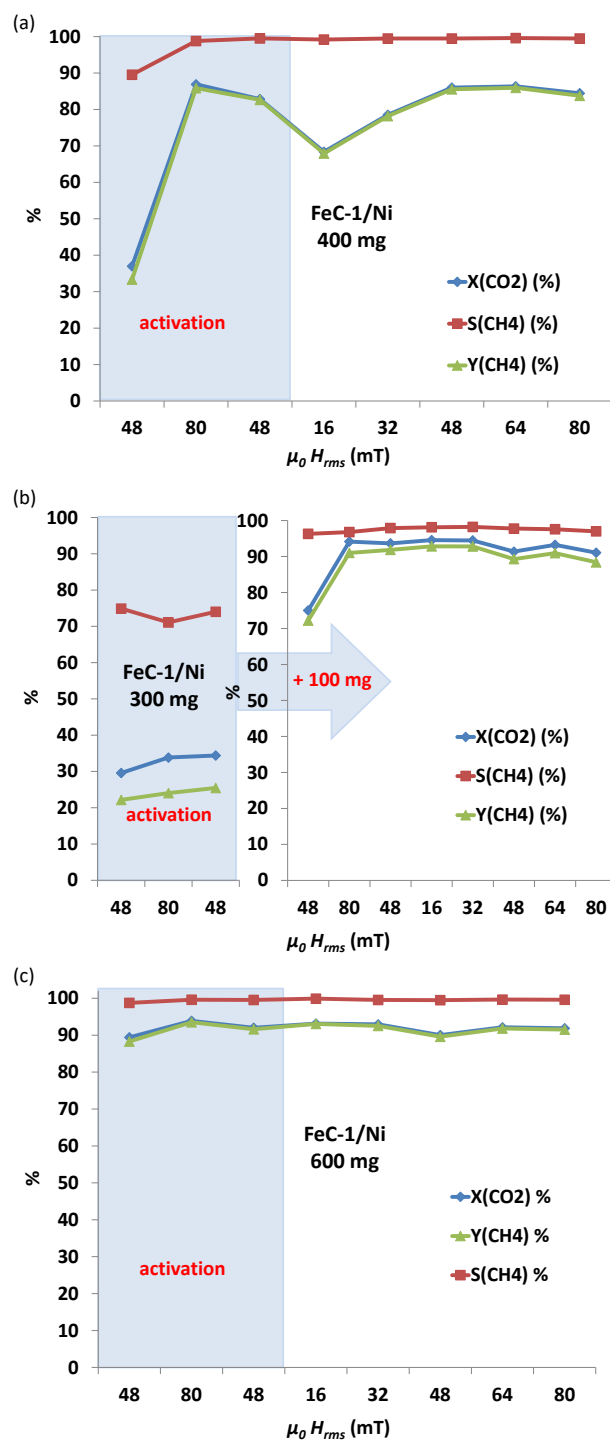


Figure S19. Magnetically induced hydrogenation of CO₂ using Fe_{2.2}C NPs **FeC-1** as heating agents. CO₂ conversion, CH₄ yield and CH₄ selectivity as a function of magnetic field when using a) 400 mg, b) 300 mg and c) 600 mg of catalyst.

ESI.9. Characterization of the catalyst *FeC-1/Ni* after the catalysis.

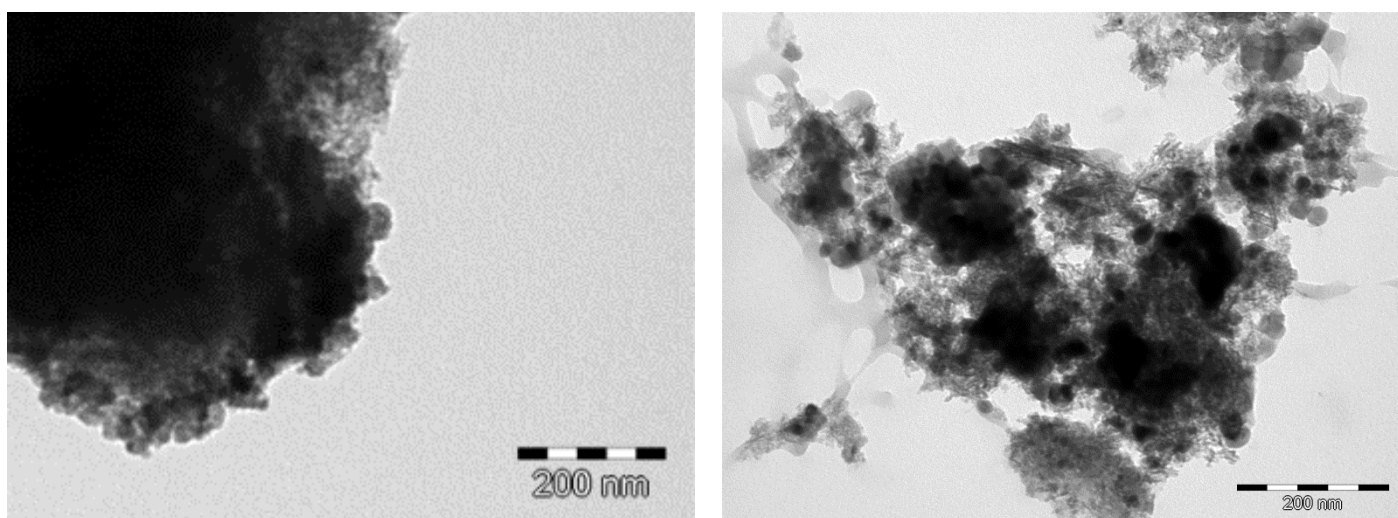


Figure S20. TEM images of *FeC-1/Ni* after catalysis when 40 mg of material were used.

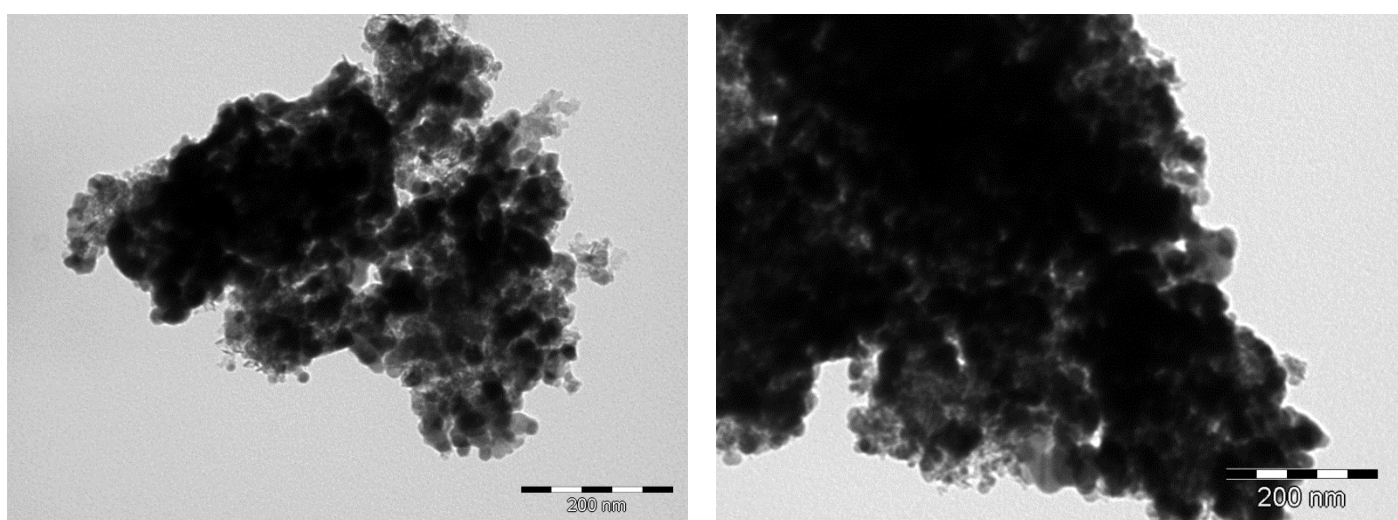


Figure S21. TEM images of *FeC-1/Ni* after catalysis when 300 mg of material were used.

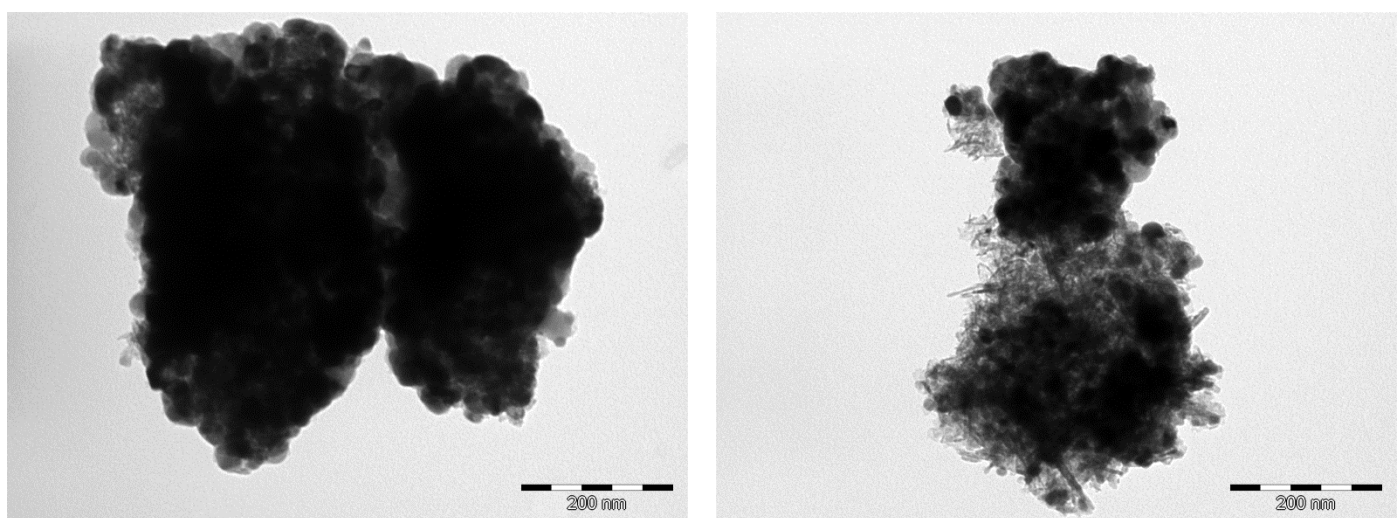


Figure S22. TEM images of *FeC-1/Ni* after catalysis when 600 mg of material were used.

ESI.10. Characterization of *Ni-pre*

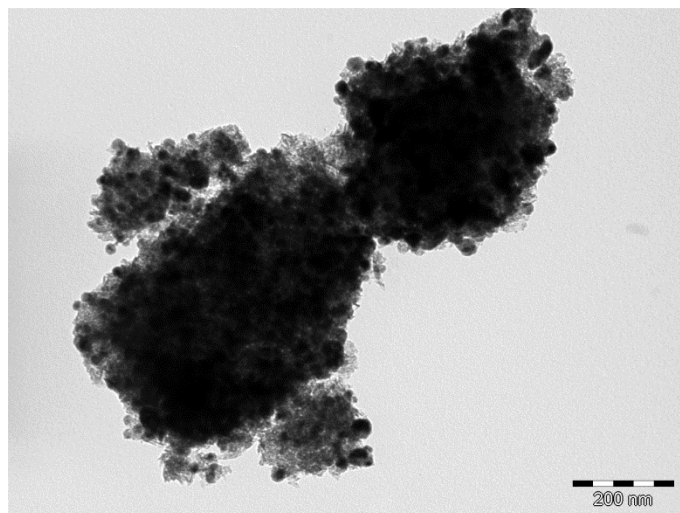
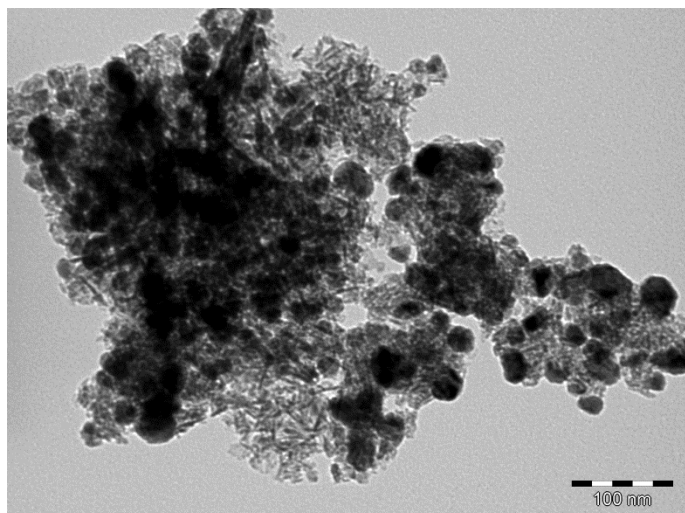


Figure S23. TEM images of **Ni-pre** at different magnifications.

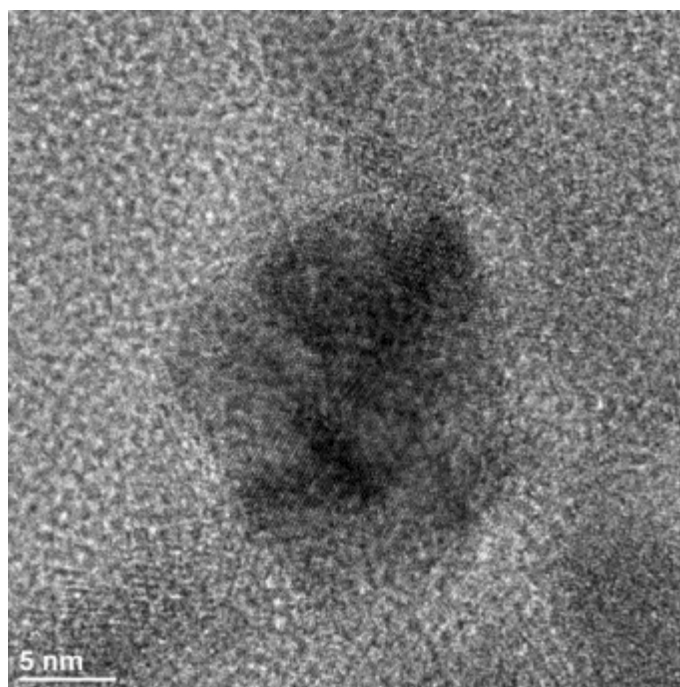
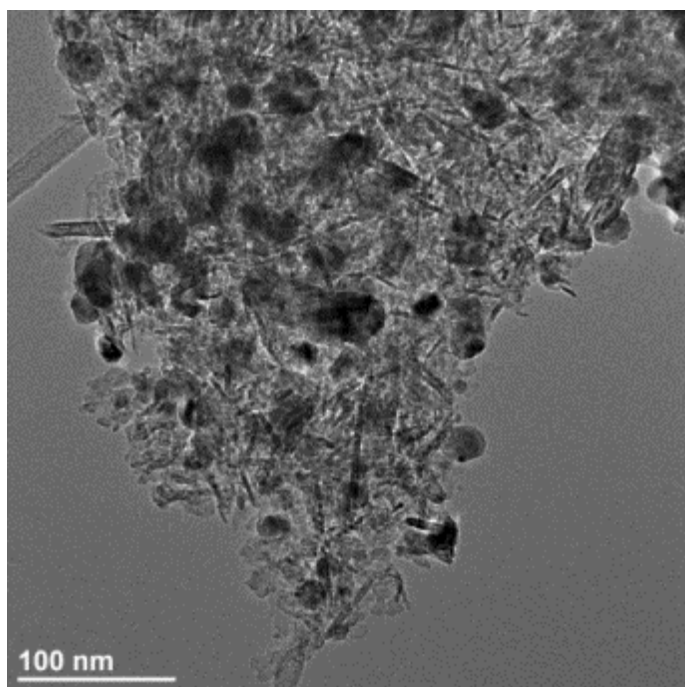


Figure S24. STEM-BF (Bright field) images of **Ni-pre** at different magnifications.

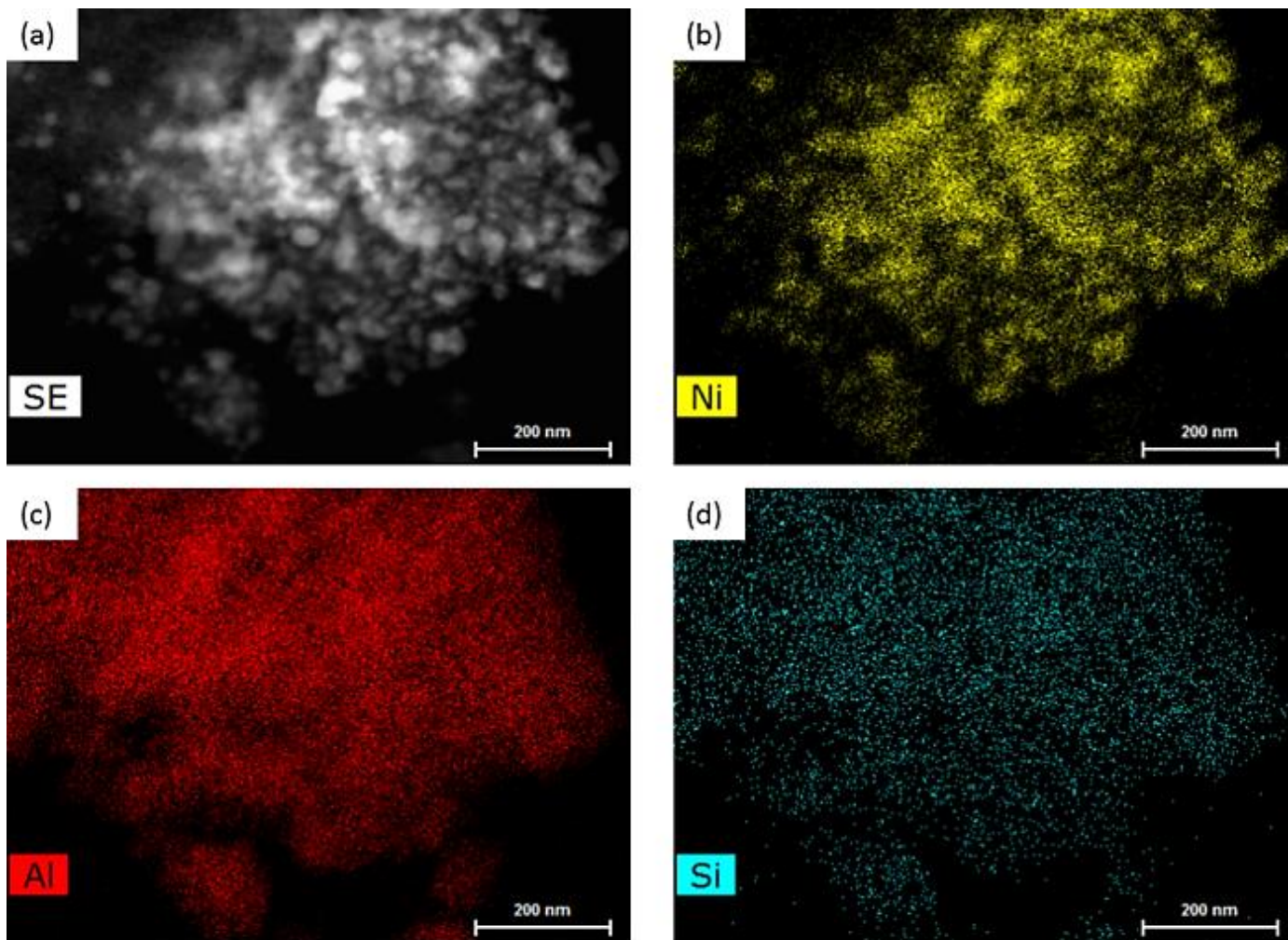


Figure S25. (a) STEM-HAADF (High angle annular dark field) image of **Ni-pre** and (b-d) EDX mapping of **Ni-pre** showing the elements (b) Ni, (c) Al and (d) Si.

ESI.11. Characterization of the catalyst *FeC-1/Ni-pre*

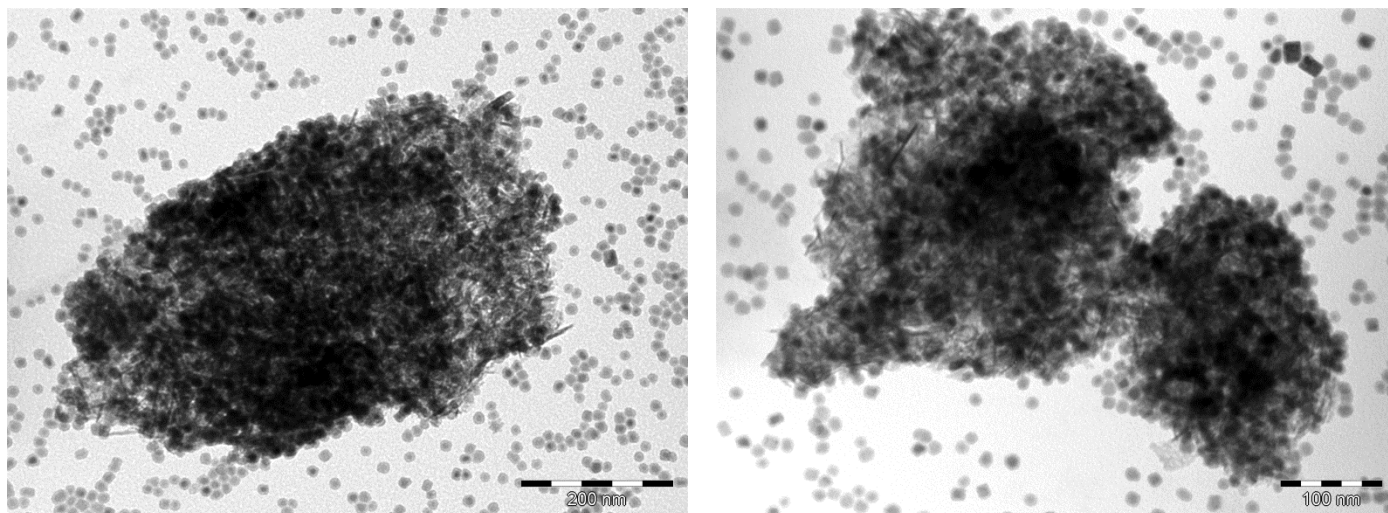


Figure S26. TEM images of *FeC-1/Ni-pre*.

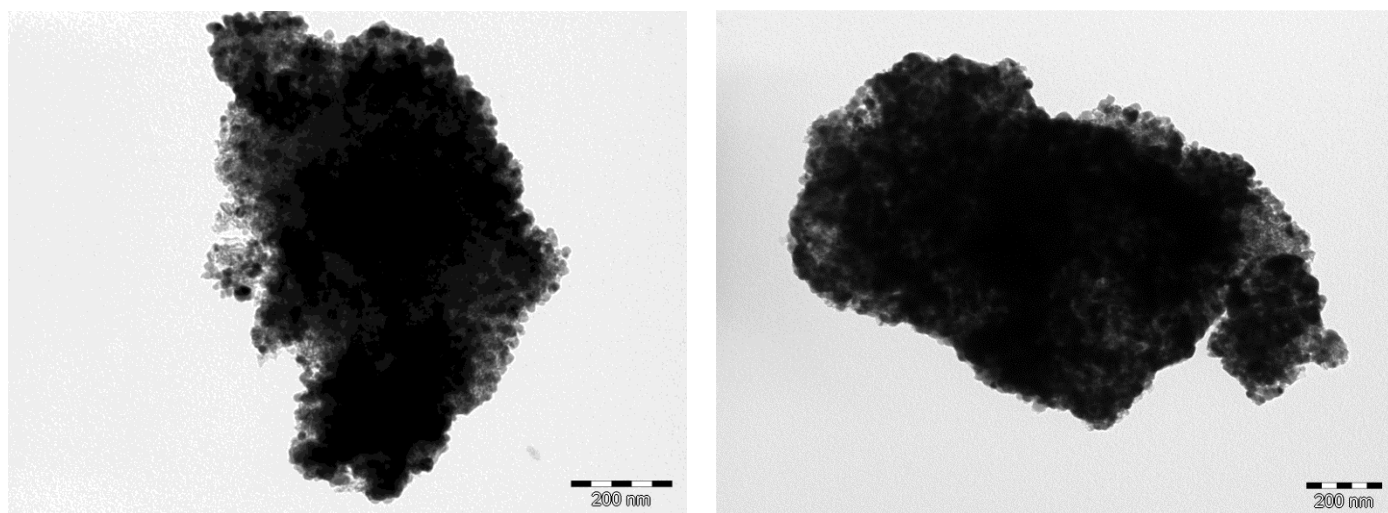


Figure S27. TEM images of *FeC-1/Ni-pre* after catalysis.

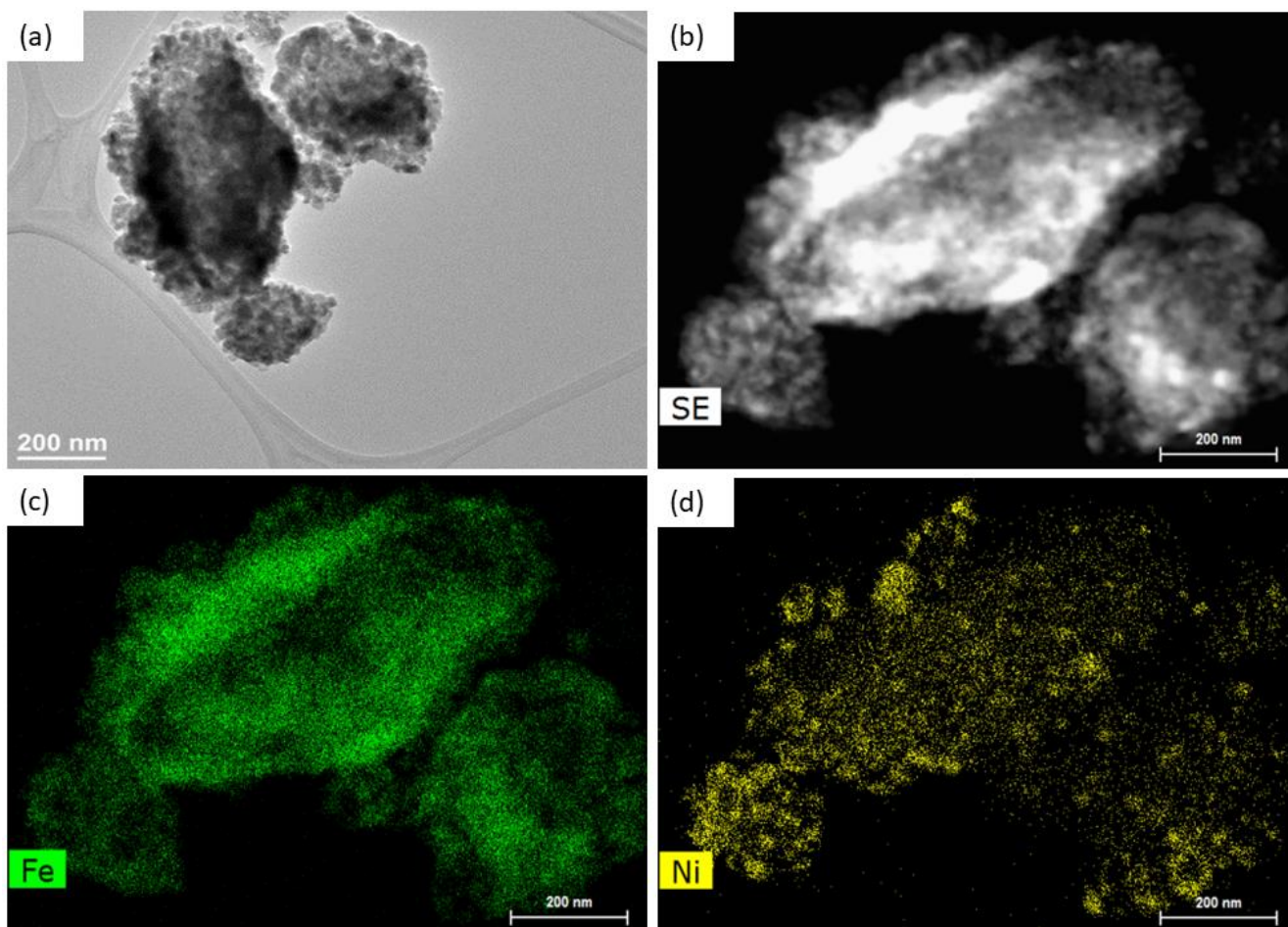


Figure S28. Characterization by HR-TEM of **FeC-1/Ni-pre** after catalysis: (a) STEM-BF (Bright field) image (b) STEM-HAADF (High angle annular dark field) and (c-d) EDX mapping showing the elements (c) Fe and (d) Ni.

ESI.12. Characterization of the catalyst *FeC-2/Ni* after catalysis

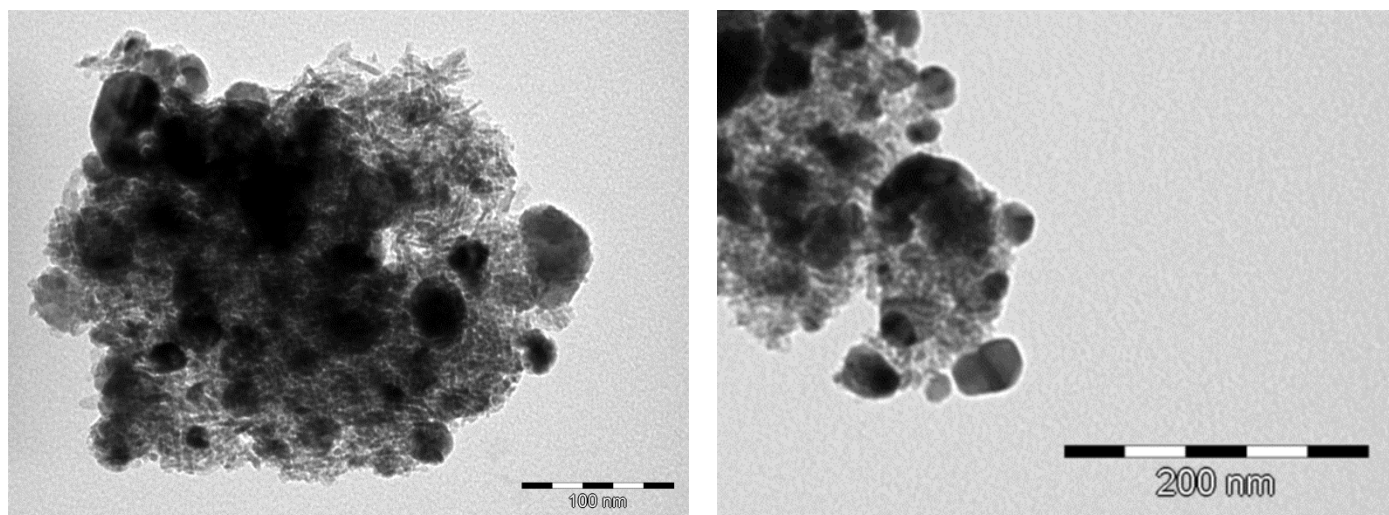


Figure S29. TEM images of *FeC-2/Ni* after catalysis.

ESI.13. Characterization of *Co/Ni* and *Co-FeC-1/Ni*

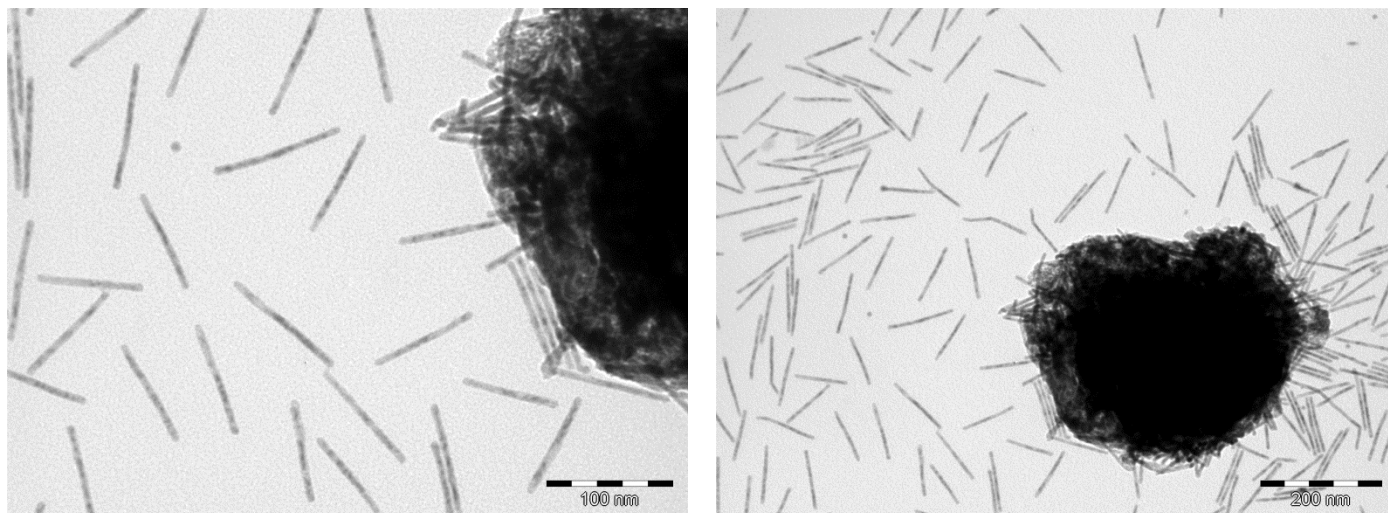


Figure S30. TEM images of *Co/Ni* at different magnifications.

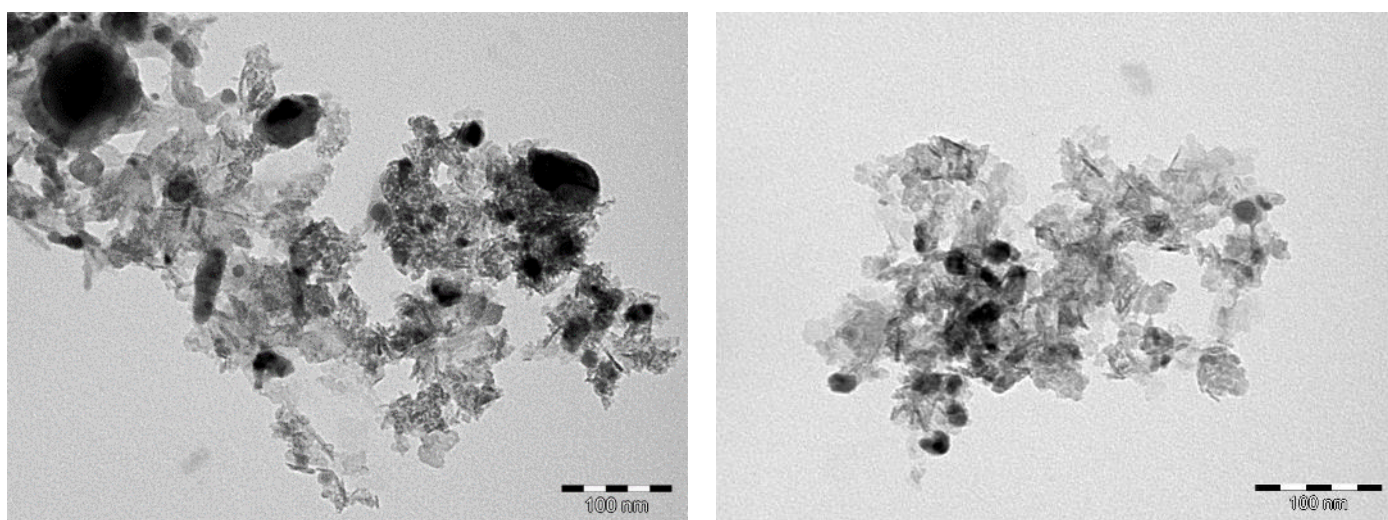


Figure S31. TEM images of *Co-FeC-1/Ni* after the catalytic reaction.

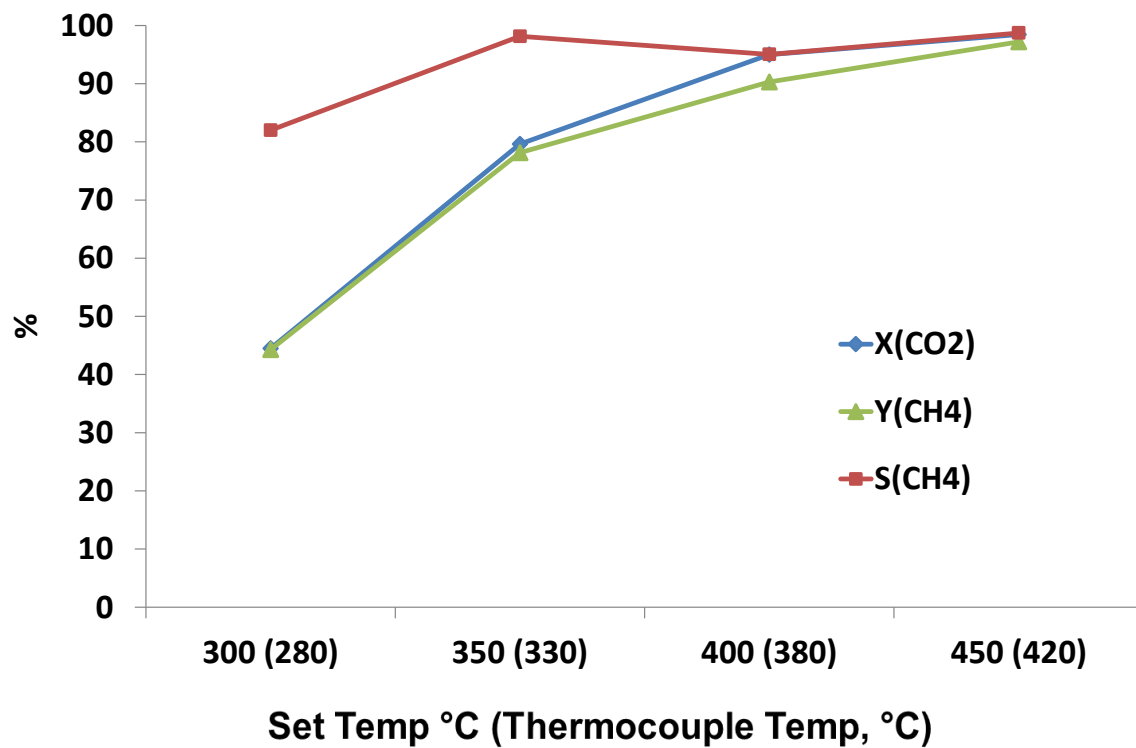


Figure S32. Catalytic results with Co-FeC-1/Ni as a function of temperature in conventional heating.

ESI.14. Image of the continuous flow reactor.

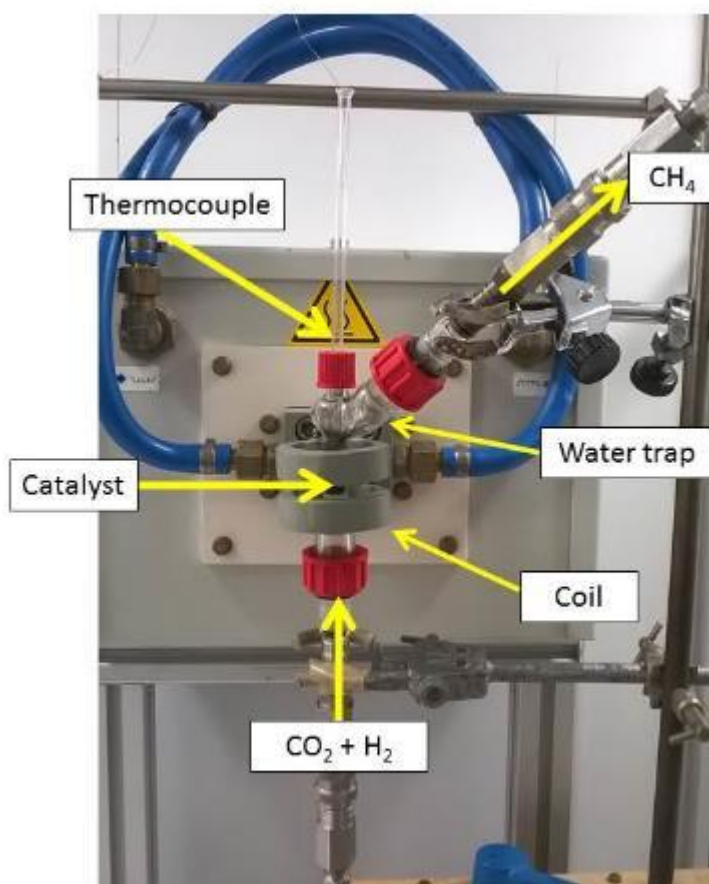


Figure S33. Schematic picture of the reactor and the coil. The thermocouple was introduced into a quartz tube which was kept in contact with the solid at the centre of the coil.

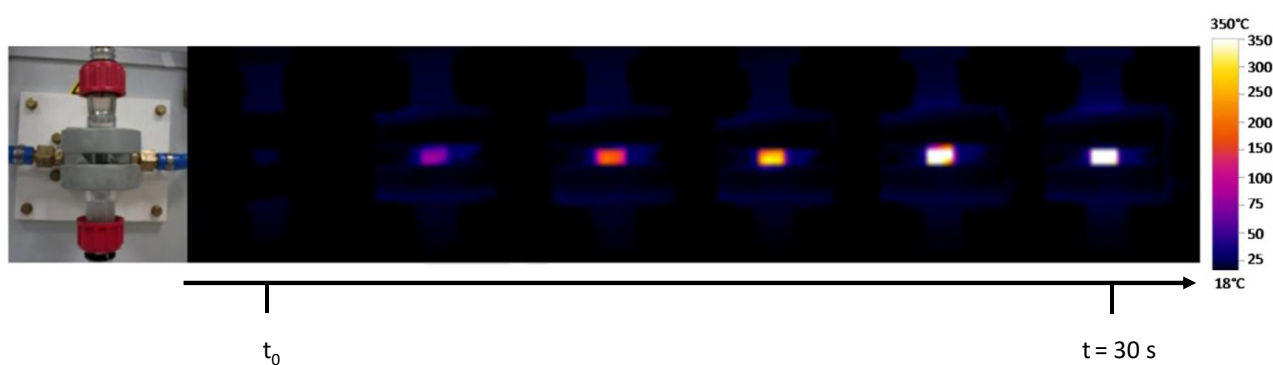


Figure S34. IR camera (*testo 885*) images showing temperatures at the reactor surface as a function of time just after application of the magnetic field.

ESI.15. Bibliography.

1. A. Bordet, L.-M. Lacroix, P.-F. Fazzini, J. Carrey, K. Soulantica and B. Chaudret, *Angew. Chem., Int. Ed.*, 2016, **55**, 15894-15898.
2. L.-M. Lacroix, S. Lachaize, A. Falqui, M. Respaud and B. Chaudret, *J. Am. Chem. Soc.*, 2009, **131**, 549-557.
3. J. M. Asensio, J. Marbaix, N. Mille, L.-M. Lacroix, K. Soulantica, P.-F. Fazzini, J. Carrey and B. Chaudret, *Nanoscale*, 2019, **11**, 5402-5411.
4. S. Lentijo-Mozo, R. P. Tan, C. Garcia-Marcelot, T. Altantzis, P.-F. Fazzini, T. Hungria, B. Cormary, J. R. Gallagher, J. T. Miller, H. Martinez, S. Schrittwieser, J. Schotter, M. Respaud, S. Bals, G. V. Tendeloo, C. Gatel and K. Soulantica, *ACS Nano*, 2015, **9**, 2792-2804.
5. M. Mikhaylova, D. K. Kim, N. Bobrysheva, M. Osmolowsky, V. Semenov, T. Tsakalakos and M. Muhammed, *Langmuir*, 2004, **20**, 2472-2477.